



Development of an Ultra Wide-Band (UWB) Synthetic Aperture Radar (SAR) System for Imaging of Near Field Object

Seyedeh Shaghayegh Fayazi

Department of Applied Physics & Electronics
UMEÅ INSTITUTE OF TECHNOLOGY
UMEÅ UNIVERSITY
Umeå, Sweden
Master of Science Thesis 2012

Master of Science Thesis.

Copyright©2012 Seyedeh Shaghayegh Fayazi.

Supervisors: Jian Yang.(SV1), Hoi-Shon Lui.(SV2), Ulrik Söderström.(SV2)

Examiner: Sven Rönnbäck.

Keywords: Bow Tie Antenna,Ultra Wideband (UWB), Synthetic Aperture Radar (SAR),
Direction of Arrival (DOA).

Technical Report No. EL 12 18.

Department of Applied Physics and Electronics,

Umeå University,

SE-90187, Umeå, Sweden. Telephone: +46 90786 50 00

October 2012.



Syedeh Shaghayegh Fayazi

Ht 2012

Master Thesis of Science, 30 hp

Master program in Robotics and Control, 120 hp

Preface

This is a technical report of my master thesis project, a part of the Master of Science degree at Umeå University. This report is the result of a one-year research collaboration between Food Radar System AB and the Department of Signals and Systems, Antenna Group, Chalmers University of Technology. My supervisors are Associate Professor Jian Yang and Assistant Professor Hoi-Shon Lui at Chalmers University of Technology, Joakim Nilsson at Food Radar System AB and Ulrik Söderström at Umeå University. Sven Rönnbäck is the examiner. This project has been financed by Food Radar System AB and Chalmers University of Technology.

This report contains results of the study of developing an Ultra Wide Band(UWB) Synthetic Aperture Radar(SAR) used in the system for near-field object detection. The algorithm system can be further enhanced for potential applications like foreign object detection in food. The intellectual property rights of this project are reserved for Food Radar System AB and Chalmers.

Acknowledgements

This thesis would not have been possible without the participation of my supervisors Associate Prof. Jian Yang and Assistant Prof. Antony Hoi-Shon Lui, not only because of their technical support and sharing their knowledge with me but also for all their kind help and guidance making the process of this thesis work easier for me. Jian and Antony, I feel privileged to work under your excellent supervision. Many thanks to my supervisor Ulrik Söderström at Umeå University for his trust and kind support during the whole period of this thesis. I would like to thanks Food Radar System AB and specially Sven-Gunnar Bodell and Joakim Nilsson to make this thesis possible. This thesis would have never seen the light without the support and collaboration with Chase Center and antenna group at the department of signal and systems, Chalmers University of Technology. I would like to thank you all the nice people in the Department of signal and systems for making many happy moments for me.

Seyedeh Shaghayegh Fayazi, Gothenburg, Sweden 2012

Dedication

*To my family;
my father Abolhassan Fayazi, my mother Bahar Tahvildari, my brother Arash, my sister
Nina and her family, Reza Atefi and his family.*

Abstract

Ultra-wideband (UWB) technology and its use in imaging and sensing have drawn significant interest in the last two decades. Extensive studies have contributed to utilize UWB transient scattering for automated target recognition and imaging purposes. In this thesis a near-field UWB synthetic aperture radar (SAR) imaging algorithm is presented.

It is shown with measurements and simulation, that it is possible to reconstruct an image of an object in the near field region using UWB technology and SAR imaging algorithm. However the final SAR image is highly affected by unwanted scattered fields at each pixel usually observed as an image artifact in the final image. In this study these artifacts are seen as a smile around the main object. Two methods are suggested in this thesis work to suppress this artifact. The first method combines the scattered field information received from both rear and front of the object to reconstruct two separate images, one from rear view and one from front view of the object respectively. Since the scattered fields from behind the object are mirrored, the pixel by pixel multiplication of these two images for objects with simple geometry will cancel the artifact. This method is very simple and fast applicable to objects with simple geometry. However this method cannot be used for objects with rather complex geometry and boundaries. Therefore the Range Point Migration (RPM) method is used along with the global characteristics of the observed range map to introduce a new artifact rejection method based on the directional of arrival (DOA) of scattered fields at each pixel. DOA information can be used to calculate an optimum theta for each antenna. This optimum angle along with the real physical direction of arrival at each position can produce a weighting factor that later can be used to suppress the effect of undesired scattered fields producing the smile shaped artifact. Final results of this study clearly show that the UWB SAR accompanied with DOA can produce an image of an object free of undesired artifact from scattered field of adjacent antennas.

Contents

List of Figures	iii
List of Tables	v
1 Introduction	1
1.1 Background	1
1.2 Company Presentation	1
1.3 Project Description	2
1.4 Project Requirement	2
1.5 Project Organization and Resources	2
2 Theory	3
2.1 Ultra Wideband Technology	3
2.2 SAR Concept	4
2.3 UWB Antenna	5
2.3.1 UWB Antenna Research at Antenna Group at Chalmers	5
3 System Setup	7
3.1 The near field UWB SAR system	7
3.1.1 Experimental setup with only one Bow-Tie antenna	8
3.1.2 Experimental setup with two Bow-Tie antenna	10
3.1.3 Experimental setup with an array of ten Bow-Tie antennas	11
3.2 Setup Calibration	12
3.3 Data Acquisition	13
3.3.1 Data preprocessing	13
4 Imaging Algorithm	16
4.1 Time Domain SAR Imaging Algorithm	16
4.2 Artifact Concept	16
4.2.1 Artifact rejection using scattered filed from behind the object	17
4.2.2 Direction of arrival artifact rejection	18

5	Result	23
5.1	Readings from VNA and Preprocessing	23
5.2	SAR Image from One Antenna	24
5.2.1	SAR image reconstructed from one antenna and a rectangular metal plate	24
5.2.2	SAR image constructed from one antenna and a U shape metal plate	26
5.3	SAR Image from Two Antennas	27
5.3.1	SAR image reconstructed from two antennas set up and a rectangular metal plate	28
5.4	Artifact Rejection	29
5.4.1	Artifact rejection using the scattered fields from behind the object	30
5.4.2	Artifact rejection using directional of arrival (DOA) information .	30
6	Conclusions and Future Work	37
6.1	Discussion	37
6.2	Conclusion	38
6.3	Future Work	38
	Bibliography	42
A	List Of Publications	43
A.1	Paper A	44
A.2	Paper B	47
B	MATLAB Codes	50
B.1	Freq. Domain to Time Domain	50
B.2	SAR Imaging	51
B.3	DOA Method	53
B.4	Optimal Theta	56
B.5	Physical Theta	56
B.6	RPM Method	56
B.7	Scattered Field	57

List of Figures

2.1	UWB communication	4
2.2	Comparison of RAR and SAR	5
3.1	Measurement General setup	8
3.2	Self-grounded Bow-Tie antenna	8
3.3	Anechoic Chamber	9
3.4	Measurement setup with one Antenna (Red path)	9
3.5	Measurement setup with one Antenna (Yellow path)	10
3.6	Measurement setup with two antennas	10
3.7	Setup with an Array of antennas, It is symmetrical over x and y axis . . .	11
3.8	Experimental setup with an array of antennas, real geometry	11
3.9	An example of time domain data from first measurement	14
3.10	An example of Time and Frequency domain data	14
4.1	SAR Geometry	17
4.2	Artefact Concept	18
4.3	Geometry of the actual antenna and rear antenna	18
4.4	Schematic of RPM method	19
4.5	Physical theta Geometry	19
4.6	Optimal theta geometry	20
4.7	Antenna 35 for pixel (29,32) where the object is present.	22
4.8	Antenna 25 for the position (26,49) where the artifact is happening . . .	22
5.1	VNA recorded data for Red path	24
5.2	VNA recorded data for Yellow path	25
5.3	Reconstructed SAR image with resolution $16mm \times 10mm$ for red path .	26
5.4	Reconstructed SAR image with resolution $16mm \times 10mm$ for yellow path	27
5.5	1D reconstructed SAR image for <i>U</i> shaped metal plate	28
5.6	SAR image reconstruction results based on the front and back antenna . .	29
5.7	The resultant image after modified the algorithm	30

5.8	SAR reconstructed image after applying DOA method	31
5.9	a) Received signal with SAR value and b) The noise is removed	32
5.10	Real geometry of U shaped metal object in yellow path when antenna is in front of the object	33
5.11	The picked value is zero	33
5.12	The picked value is non zero	33
5.13	Reconstructed SAR image after applying Threshold and scanning the pixels	34
5.14	Five pixels in the column in front of one antenna where the object is present are picked	34
5.15	Three pixels in the column in front of one antenna where the object is present are picked	35
5.16	SAR reconstructed final image	35
5.17	SAR reconstructed image from simulated data	36

List of Tables

3.1	Calibration properties for one and two antennas setup	12
3.2	Calibration properties for an array of the antennas setup	12

1

Introduction

1.1 Background

Foreign object detection in food has always been in center of attention for food industry especially in the packaging section. Many detection technologies have been established during last few years but still low-density foreign bodies like plastic, wood and fruit stones are invisible for the traditional detection methods. A solution to this problem can be the use of Ultra Wide-Band and Synthetic Aperture Radar imaging. As UWB technology uses a large frequency band and pulses, it has many advantages over the traditional narrow band counterpart, It has good penetration ability , higher resolution, ability to detect slowly moving objects and much simpler system configuration. Beside that the concept of SAR imaging has been well known and widely applied to various remote sensing applications. It is believed this combination can fit high resolution foreign object recognition requirement in food industry

1.2 Company Presentation

Food Radar System AB is a company located in Gothenburg, Sweden, focusing on new methods for the detection of foreign bodies in food packaging industry. Food Radar Systems started as a joint research project together with the industry and Chalmers University of Technology at SIK - The Swedish Institute for food and biotechnology. The latest safety technology developed by Food Radar System AB [1] is called LOOK100* which is a sensor designed for emulsions and pump-able products. This system has the ability to detect foreign bodies like metal, stone and glasses, it is also suitable for detecting wood, plastic, bone and even insects that up to now have gone undetected. Now the company is focusing on development of a new algorithm for detection of foreign

objects in solid food e.g cheese that is moving slowly on a conveyer belt.

1.3 Project Description

Food Radar System AB is aiming to develop an algorithm for detection of foreign bodies within a solid food like cheese that is slowly moving on a conveyer belt. As it was briefly explained earlier and you will read in the rest of this report UWB in synthetic aperture mode is a very strong candidate for such purpose. In the first phase of the project SAR algorithm [2] for the reconstruction of an object image using only one antenna is implemented then the artifact associated with this image reconstruction method are tried to be suppressed. In the next phase of the project the algorithm will be extended from one antenna to an array of antennas for detecting objects like wood metal or plastic.

1.4 Project Requirement

The project requires a simple test setup consisting of two self grounded bow tie antennas[3, 4]. A metal object and a network vector analyzer to record the scattered field from the object. All the test setup should be built up in anechoic chamber [5] to minimize reflection from surrounding, the rest of the project will focus on developing the SAR imaging algorithm in Matlab based on recorded scattered field from the object. Once the algorithm and setup are implemented and tested an array of antennas consisting of ten bow tie antennas is built to be placed on a conveyer belt for the second phase of the project.

1.5 Project Organization and Resources

The first phase of the project which is the subject of this thesis project including the literature study, building the test set up and developing the SAR imaging algorithm were all performed in antenna group laboratory in the Department of Signals and Systems at Chalmers University of Technology under the supervision of Associate Prof. Jian Yang and Assistant Prof. Antony Hoi-Shon Lui, the second phase of the project that is focusing on developing the algorithm on an array of antennas will be performed in Food Radar System AB laboratory in SIK under the supervision of Joakim Nilsson the CTO of Food Radar System AB with regular meeting with Associate Prof. Jian Yang.

2

Theory

2.1 Ultra Wideband Technology

Ultra-wideband (UWB) is a radio technology that covers a large band width. This wide-band gives UWB many unique advantages compared to the narrow band counterpart. The large band width in the frequency domain gives the possibility of using pulses or waveforms compressed in the time domain and since the pulse energy in the frequency domain is spread in a broad range to very low level UWB radios can share spectrum with narrow band broadcasters without any interference, see Fig 2.1 On the other hand as it is observed by (2.1) the wider signal band width (BW) is, the finer range resolution (R_{res}) of the radar [6]. Therefore since UWB covers a larger bandwidth and has low center frequency it has good range resolution [7], C is the velocity of electromagnetic signal in vacuum, one benefit with this better range resolution is that signals with low frequency can penetrate a medium better. This property makes UWB a very convenient solution in target recognition applications like foreign object detection in food that the signal itself should have no impact on the quality of the material.

$$R_{res} = \frac{c}{2BW} \quad (2.1)$$

Unlike the conventional systems UWB transmits information by generating energy at certain intervals and embracing a large band width thus enabling pulse positioning or time modulation. UWB can be used at a very low energy level for short-range, high-bandwidth communications, using a large portion of the radio spectrum [8]. UWB has traditional applications in non-cooperative radar imaging, but in the last two decades UWB technology has been significantly used in imaging and automated target recognition purposes[2]. In these applications transient scattered fields of UWB are used for either imaging or target recognition [9]. As an instance Vitebskiy *etal* have shown that Ultra Wideband short pulse radar can be used to detect objects on top of the soil or

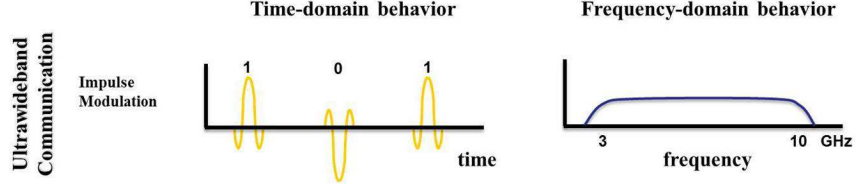


Figure 2.1: UWB communication

buried in the soil [10]. Since depending on objects physical and dielectric properties each object has its own set of resonant frequencies using UWB one object can be distinguished among a library of similar objects [11]. From a radar point of view UWB advantages can be summarized as

- Higher range resolution
- Higher penetration ability through lossy material
- Enhanced target recognition
- Immunity to passive interference (i.e., rain, fog, clutter)
- Ability to detect slowly moving or stationary targets
- Much simpler system configuration
- Lower cost

2.2 SAR Concept

If an antenna moves to cover a synthetic aperture a Synthetic Aperture Radar (SAR) is produced. SAR is a high resolution radar imaging technique achieved by collecting data along a synthetic aperture. One of the potential benefits of SAR is its finer resolution compared to a case of real aperture. In order to better understand the mechanism of a synthetic aperture we need to define some terms first. The resolution from the radar to target region along the line of sight (LOS) is called range resolution and the resolution along the direction perpendicular to the LOS and parallel to the ground is called crossrange or along-track resolution which is initially achieved by use of narrow beam. The beam width θ_B of an aperture radar is given by wavelength λ divided by the aperture diameter D , cross range resolution at range R is given by (2.2) however if an aperture length equals to the path length (synthetic aperture) L_{SA} (2.2) can be changed in to (2.3) where $\Delta\theta$ is the synthetic aperture angle, i.e the angle subtended by the synthetic aperture as seen from the target area, and the factor of two in the denominator appear due to SAR processing, therefore comparing (2.2) and (2.3) one can clearly see a super improvement of the resolution in SAR. Fig 2.2 shows a comparison between real aperture radar and synthetic aperture radar.

$$\delta_{cr} \approx \frac{R\lambda}{D} \quad (2.2)$$

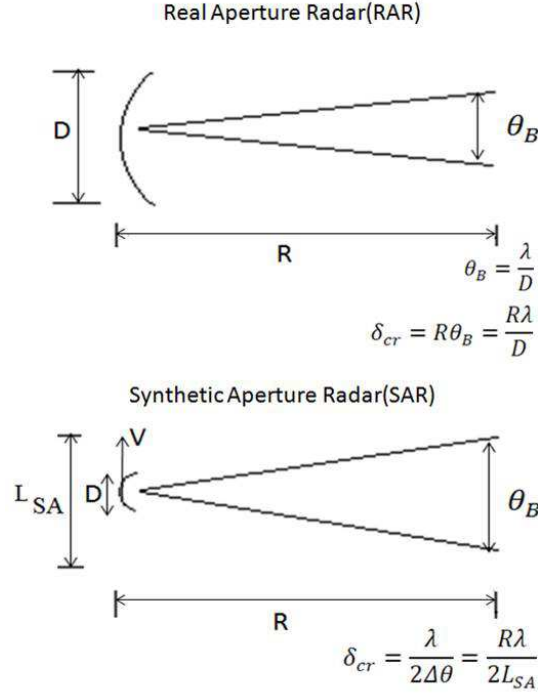


Figure 2.2: Comparison of RAR and SAR

$$\delta_{cr} \approx \frac{R\lambda}{2L_{SA}} \approx \frac{\lambda}{\Delta\theta} \quad (2.3)$$

A problem that exists with radar applications is that echoes from the surfaces or inhomogeneities will compete with scattered field returning from the object, to minimize this effect the resolution of the radar image (in slant-range and cross-range) should be matched to the size of the target. Ultra-wideband radar can match the slant-range resolution to target size, excite resonances of interest, and give useful penetration into the object. SAR processing has also the potential to match cross-range resolution to target size.” [2]. This all makes UWB in the synthetic aperture mode an ideal choice for object detection and imaging applications [2]. In this thesis work we aim to introduce a setup for imaging the near field objects using UWB in synthetic aperture mode.

2.3 UWB Antenna

2.3.1 UWB Antenna Research at Antenna Group at Chalmers

UWB antenna research has been emphasized for years at Antenna Group at Chalmers University of Technology. Many contributions to UWB antennas have been achieved.

The Eleven antenna, a decade bandwidth antenna, has unique characteristics: the nearly constant beamwidth, the fixed phase center location, high aperture efficiency, good reflection coefficient, all over a decade bandwidth [12]–[21]. The main application of the Eleven antenna is as a feed for reflector antennas for future radio telescopes. In addition, the Eleven feed can also be used in other applications, such as UWB MIMO antenna [22, 23], monopulse tracking antenna [24], TV antenna [25] and dual-band antenna [26].

The self-grounded Bow-Tie antenna is the antenna used in this project. It can be used in many UWB systems, especially in short pulse systems, such as in medical applications [27] and indoor UWB radar system[28].

The hat-fed reflector antenna can also be considered as a wideband antenna, which finds many applications in communication systems [29]–[34] and gauge tank radars.

There are also other antenna research at antenna group, such as the base station antenna for wireless communication systems [35]–[37].

3

System Setup

3.1 The near field UWB SAR system

In order to use UWB imaging technique for near field region object detection, as it is the case of this project the general setup shown in Fig 3.1 is used. this setup consist of an object and an array of antennas. the object is then moved along a conveyer belt. This setup can be limited to only one antenna which is a monostatic system and the antenna is acting as both transmitter and receiver (reflection-sensing), or two antennas which is bistatic (reflection- and through sensing) system or an array of antennas.

Among many available choices for antenna, self-grounded Bow-Tie antenna is used, see Fig 3.2. Self-grounded Bow-Tie antenna is chosen since it is a compact and simple small antenna with low profile and directional UWB radiation characteristics [3, 4]. With simulation and measurements Yang has shown some properties of the UWB Bow-Tie antenna, such as -10 dB reflection coefficient, stable radiation patterns over the frequency range of 2-15 GHz and a good time domain response [3]. It has also been shown that the Bow-Tie antenna is superior to some alternative choices like Vivaldi in terms of penetration ability [4]. These properties make self-grounded Bow-Tie antenna an ideal choice for ultra wide band SAR imaging of near filed objects.

The entire measurement should be performed in an anechoic chamber equipped with absorber on all the walls, so that the reflections from surroundings are minimized, see Fig 3.3. [5]. It is important to note that in order to increase the accuracy of the measurement especially in the first and second setup it is important that the antenna and the cables are fixed so the measurement error due to the movement of cables is minimized.

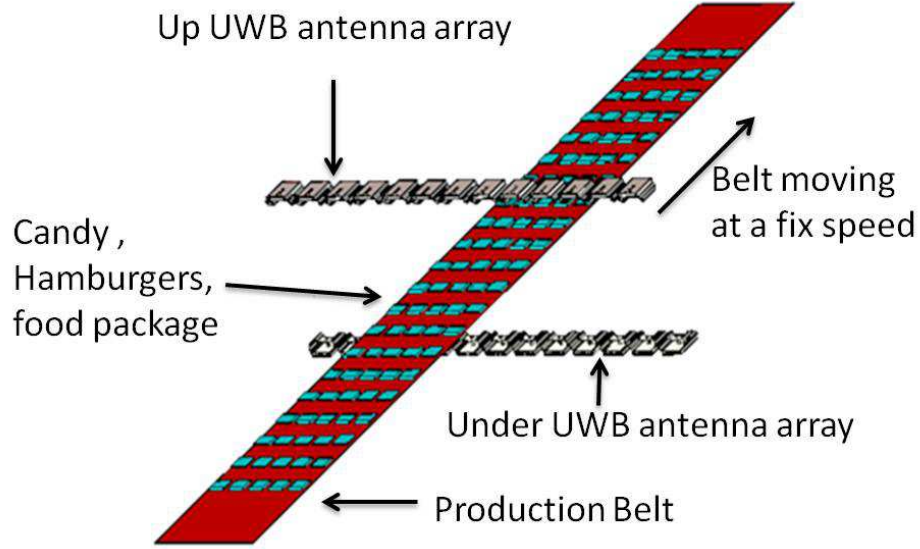


Figure 3.1: Measurement General setup



Figure 3.2: Self-grounded Bow-Tie antenna

3.1.1 Experimental setup with only one Bow-Tie antenna

In the first step only one Bow-Tie antenna is used acting as both transmitter and receiver. However to produce the same geometry and effect as an array of antenna the object is moved in front of this single Bow-Tie antenna. See Fig 3.4. This will give us multiple views of the object which is placed in 68 equal-spaced positions along a straight line of 1088 mm long. In order to have a high flexible and accurate positioning system for the measurement at a low cost in this study, this straight path of 1088 mm long was built up of 68 Duplo LEGO blocks at two different distances from the antenna, one

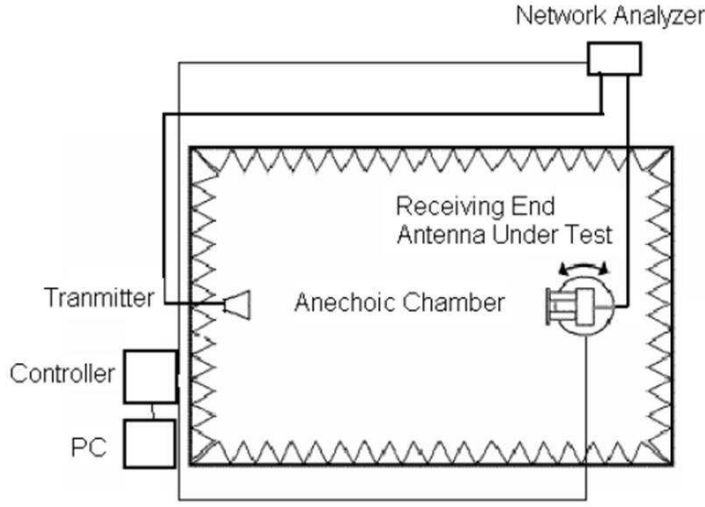


Figure 3.3: Anechoic Chamber

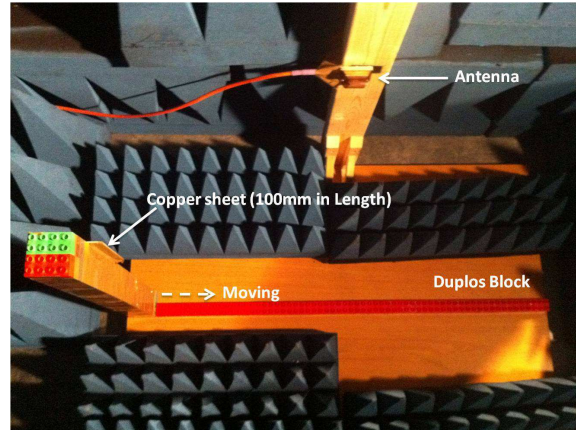


Figure 3.4: Measurement setup with one Antenna (Red path)

in red and the other in yellow see Fig 3.4 and 3.5. The monostatic responses at each of these 68 positions are measured using a PNA Network Analyzer - model of E8363B 10MHz-40GHz - in the frequency range of 0.5 GHz to 13 GHz.

As shown in Fig 3.4 and 3.5 each Duplo block has a length of 16mm , and the distance between the antenna and the LEGO path is 385mm for the red path, and 715mm for yellow path. The objects used for this set up are a rectangular and a *U* shaped metal plate.

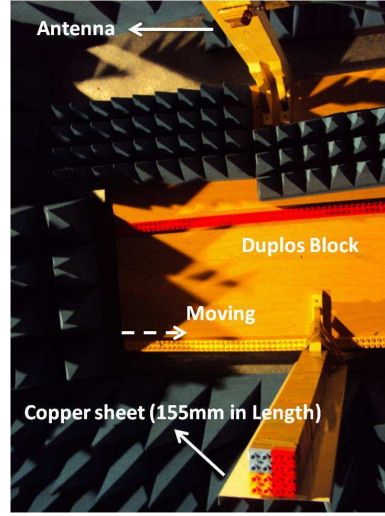


Figure 3.5: Measurement setup with one Antenna (Yellow path)

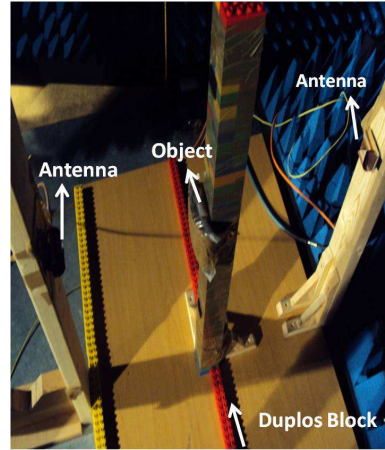


Figure 3.6: Measurement setup with two antennas

3.1.2 Experimental setup with two Bow-Tie antenna

In the second step another Bow-Tie antenna is added to the previous setup so that the transmitter and receiver antenna are separated. This will provide us with bistatic responses from the object. Using two antennas we will have the possibility to have scattered fields information from rear and front of the object. The schematic of this set up is presented in Fig 3.6

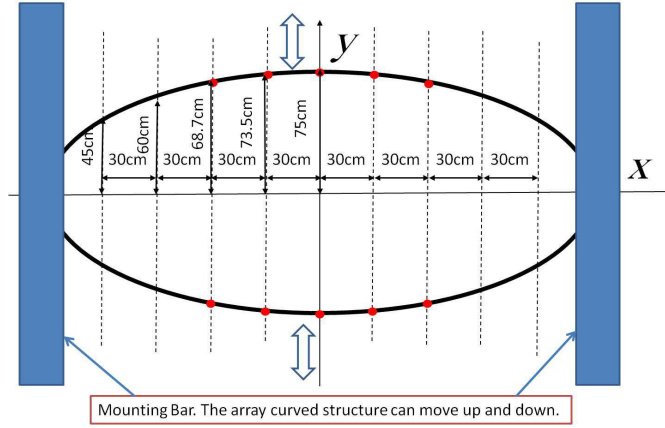


Figure 3.7: Setup with an Array of antennas, It is symmetrical over x and y axis

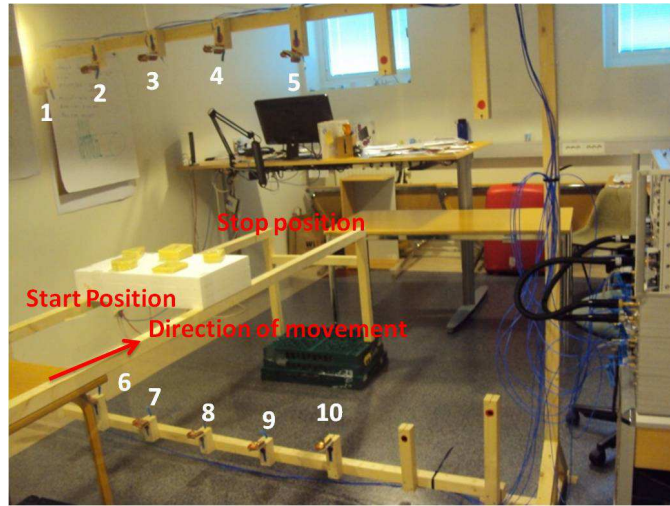


Figure 3.8: Experimental setup with an array of antennas, real geometry

3.1.3 Experimental setup with an array of ten Bow-Tie antennas

In the third measurement setup, number of antennas is increased from two to ten. In this set up five antennas are allocated to the front of the object and five to its rear, see Fig 3.7 and 3.8. This new setup will give us a higher resolution of bistatic response from object, finally helping us to construct a better image from inside the object.

3.2 Setup Calibration

For the first and second measurement setup in order to calibrate the network vector analyzer, ports are connected to Electronic calibration module model $-N4431-60006-300kHz-13.5GHz$, with the following setting listed in table 3.1

Table 3.1: Calibration properties for one and two antennas setup

Start Frequency (GHz)	Stop Frequency (GHz)	Number of Samples	if Bandwidth (Hz)
0.5	13	6401	150

For the third setup Electronic calibration module model $-85093-60010-300kHz-9GHz$ is connected to Network vector Analyzer ports with the following setting listed in table 3.2

Table 3.2: Calibration properties for an array of the antennas setup

Start Frequency (GHz)	Stop Frequency (GHz)	Number of Samples	IF Bandwidth (Hz)	Power (dBm)
1.5	9	1601	600	7

3.3 Data Acquisition

As explained earlier all the measurements are performed in an anechoic chamber using a Network vector Analyzer. NVA will provide us with recording in both time and frequency domain. The frequency measurements are recorded in the frequency range $0.5 - 13GHz$ for the one and two antennas setup and $1.5 - 9GHz$ for the array of antennas, each with 6401 and 1601 samples respectively. NVA uses Chirp Z transform [38] to provide us with measurements in time domain. Measurements in time domain are between $-10nS$ to $+10nS$, see Fig 3.9. However, we can use inverse Fast Fourier transform (3.1) to obtain time domain data from frequency domain data. In digital system the data $U(j\omega)$ consists of a finite Number N of samples U_n and it gives us the inverse Discrete Fourier Transform ($IDFT$) (3.2) The absolute value of time and frequency is depended on the number of samples N and the sample frequency f_T , (3.3)

$$u(t) = \frac{1}{2\pi} \int_{-\infty}^{+\infty} U(j\omega) e^{j\omega t} d\omega \quad (3.1)$$

$$u_k = \frac{1}{N} \sum_{n=0}^N U_n \cdot \exp(j \cdot k \frac{2\pi \cdot n}{N}) \quad (3.2)$$

$$\Delta f = \frac{1}{N \cdot \Delta t} = \frac{f_T}{N} \quad (3.3)$$

where Δt is interval between time samples and Δf is the interval between frequency samples. It is important to note that a Bicycle window (3.4) should be used on data prior to inverse fast Fourier transform.

$$W_b(f) = (\omega t_i)^4 e^{-\omega t}, \omega = 2\pi f \quad (3.4)$$

An example of data converted from frequency to time domain is presented in Fig 3.10. It is clearly seen that the data converted from frequency to time (blue) follows the time data (red). Later on it will be seen that since SAR imaging algorithm requires time domain data and in the case of array of antennas we only have frequency data it is necessary to transfer frequency data into the time domain

3.3.1 Data preprocessing

The reflection from the antenna itself that is usually seen as a big beam in time domain data, see Fig 3.9, is time gated out over the data set. However time gating will produce a delay that must be taken in to account when reconstructing the final image. This time delay will be seen as a distance calculated by (3.5) where c is the speed of light. Later on this distance will be added to all values participating in image reconstruction using SAR algorithm

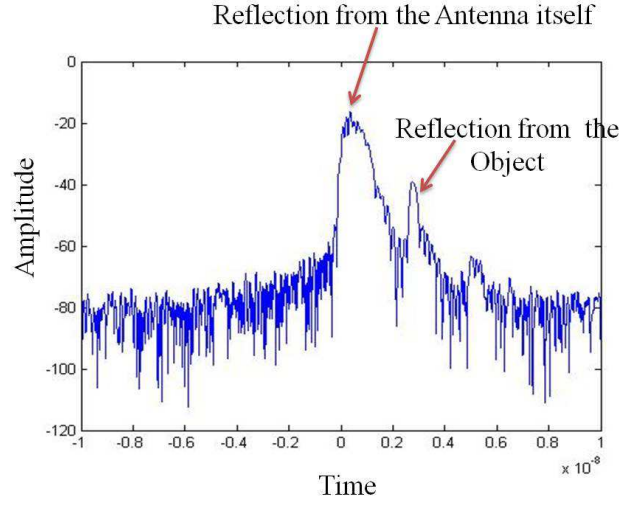


Figure 3.9: An example of time domain data from first measurement

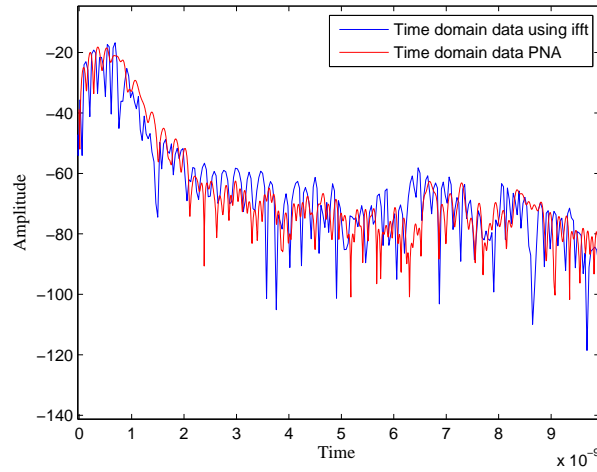


Figure 3.10: An example of Time and Frequency domain data

$$t = \frac{2 \times d}{c} \quad (3.5)$$

It is important to note that the amplitude of the measured data from VNA is in dB and all the measurements are converted into the linear scale using (3.6).

$$L_{dB} = 20 \log_{10} \left(\frac{A_1}{A_0} \right) \rightarrow A_1 = (10)^{\frac{L_{dB}}{20}} A_0 \quad (3.6)$$

Where A_1 is measured amplitude and A_0 is reference amplitude

4

Imaging Algorithm

4.1 Time Domain SAR Imaging Algorithm

The Geometry of SAR is shown in Fig 4.1. In order to construct an image of an object, scattered fields from the object at each position are recorded with VNA, then these scattered fields are used to construct the final image using SAR imaging mathematical equation (4.1) [2].

In this method, the distance between the antenna array and the object is known and included in the imaging algorithm, Fig 4.1. First, the propagation delay from each point in the scene (i.e. the image/ area of interest) to each antenna is computed, then scattered fields in the time domain are measured at the antenna. Finally, the SAR image is constructed. The intensity of each pixel $I(m,n)$ is given by (4.1)

$$I(m,n) = \sum_{k=1}^K S_k(t = T_{k,m,n}). \quad (4.1)$$

In (4.1): K is the total number of the Antenna $s_k(t)$ Represents the time domain scattered field received at the k_{th} sensor position $T_{(k,m,n)}$ Is a round-trip time delay between the k sensor position and the physical position represented by pixel (m,n) on the image.

4.2 Artifact Concept

One limitation within SAR imaging algorithm is that scattered fields from adjacent antennas at each position produce undesired blurry image around the main object. To be more precise in the SAR imaging algorithm at each position the distance d between

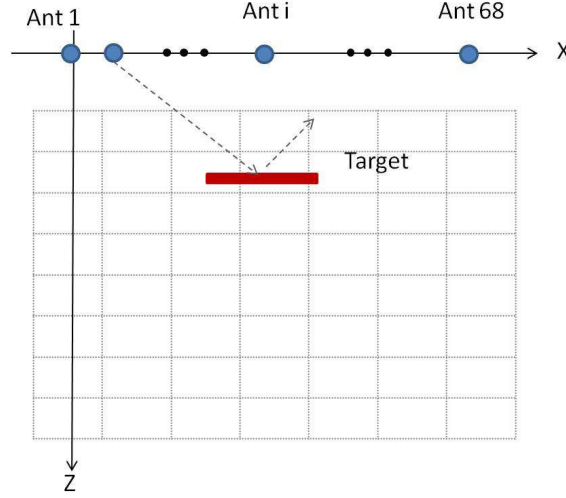


Figure 4.1: SAR Geometry

each antenna and pixel is calculated, using this distance the round-trip delay $t_d = 2d/c$ that takes for the signal to travel between antenna and pixel is calculated. based on this time the relevant SAR $S(t = t_d)$ value is picked up. If the object is presented, a strong signal $S(t = t_d)$ will be picked up and used for image reconstruction for this pixel. However, the same value is also picked up for other pixels with the same distance away from the same antenna position, see Fig 4.2. As you can see in this figure there are some other pixels with the same distance to antenna that there is no object available in them but since SAR algorithm is only based on the distance it can not determine in which of these pixels the object is presented so SAR algorithm will assign the same value to all of these pixels and this will result in the final artefact covering the main object [9]. In the case of this study this artifact is mainly observed as a smile arc around the object.

4.2.1 Artifact rejection using scattered filed from behind the object

Placing either one or an array of antenna behind the object can produce a similar image as the one reconstructed from the antennas in front of the object with only this difference that the artifact originated from scattered field of adjutant antennas is mirrored horizontally, see Fig 4.3. Multiplying these two images pixel by pixel can cancel the artifact. We have tested this method for simple object like rectangular metal plate that is also horizontally symmetric. However in more complex images that are not also horizontally symmetric this multiplication will result in the modification of the original object too, therefore it is necessary to look for better artifact compensation solution. However the simplicity and high speed of this method makes it an ideal option for the cases that the object does not have a complex geometry.

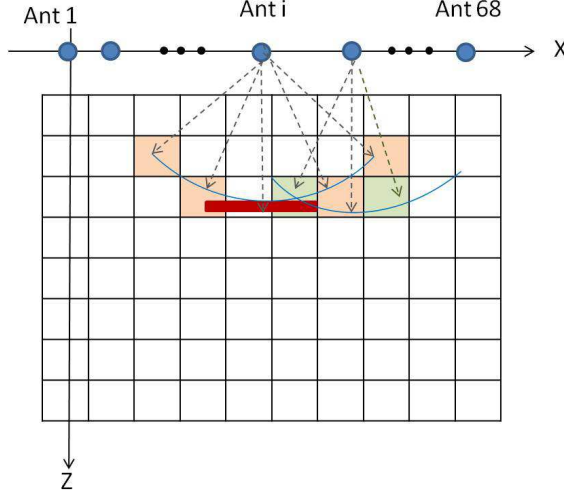


Figure 4.2: Artefact Concept

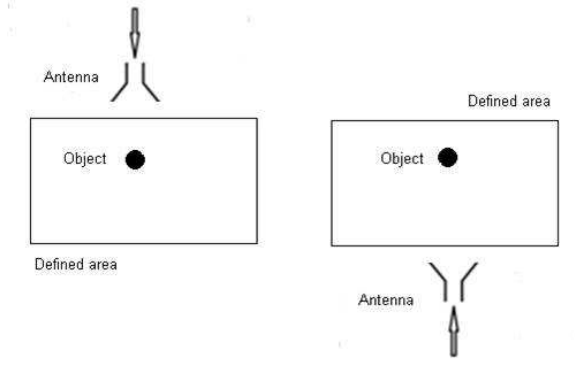


Figure 4.3: Geometry of the actual antenna and rear antenna

4.2.2 Direction of arrival artifact rejection

Another method to suppress this smile shaped artifact can be achieved using the information regarding the direction of arrival of the scattered fields at each pixel. One of the most promising algorithms for imaging different objects with rather complex boundaries is the Range Point Migration (RPM) method [39]. This algorithm assumes that any boundary point (x, z) is on a circle with the center $(X, 0)$ and radius r , see Fig 4.4. using this information an accurate Direction Of Arrival (DOA) method can be employed along with the global characteristics of the observed range map [39] to calculate an optimum theta (θ_{opt}) for each antenna. This information along with the real physical direction

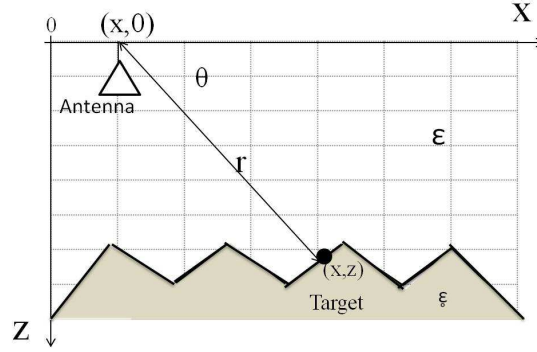


Figure 4.4: Schematic of RPM method

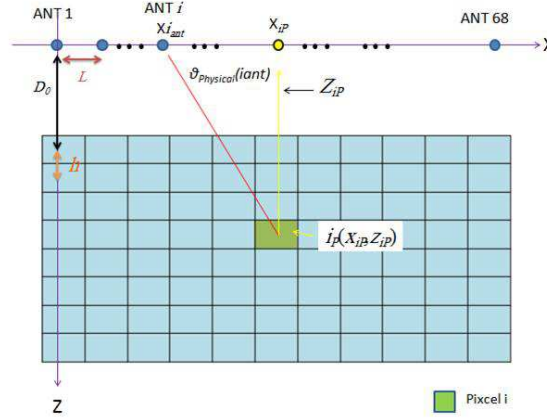


Figure 4.5: Physical theta Geometry

of arrival at each position can produce a weighting factor that can be later on used to suppress undesired scattered fields producing the smile shaped artifact.

Physical theta

For each position we can calculate an angle known as physical theta ($\theta_{physical}$). As it is shown in Fig 4.5 this angel comes from the physical distance of each pixel to the antenna (4.2)

$$\theta_{physical} = \arctan \frac{Z_{iant} - Z_{ip}}{X_{iant} - X_{ip}} \quad (4.2)$$

In Fig 4.5 D_0 is exactly when the time gating is happened and it is equal to $D_0 = (t_0 \times C)/2$, $L = 16mm$, $H = 10mm$ and to avoid minus value all value of theta are

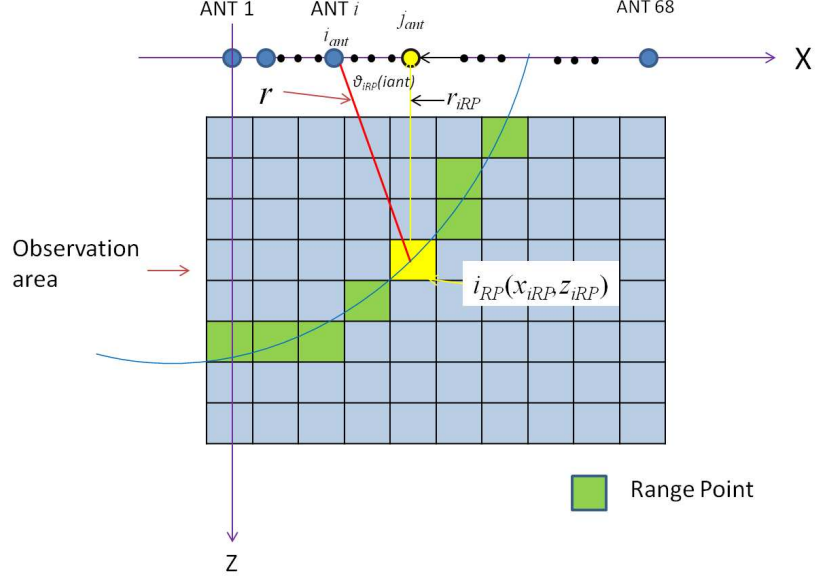


Figure 4.6: Optimal theta geometry

shifted $\pi/2$

Optimal theta

As it was mentioned earlier an accurate Direction Of Arrival (DOA) method can be employed using the global characteristics of the observed range map [39] to calculate the optimum theta (θ_{opt}) from (4.3)

$$\theta_{optimal}(i_{ant}, r) = \left(\arg \max_{0 < \theta < \pi} \left| \sum_{i_{RP}=1}^{N_{RP}(i_{ant}, r)} s_{j_{ant}}(r_{iRP}) \cdot \exp \left[-\left[\frac{(x_{i_{ant}} - x_{iRP})^2}{2\sigma_x^2} + \frac{(\theta - \theta_{iRP}(i_{ant}))^2}{2\sigma_\theta^2} \right] \right] \right| \right) \quad (4.3)$$

The amplitude of scattered field for each antenna at each position will produce an optimal theta coming from a number of range points maximizing equation (4.3), see Fig.4.6.

Range point

For each pixel there is a distance from antenna to that pixel which is shown by r , all points with the distance $r - 1mm < r < r + 1mm$ from that antenna are considered as range points for that antenna, See Fig 4.6.

Theta Range Point

Each range point is associated with an angel called $\theta_{RangePoint}$. This angel is calculated using (4.4). Again to avoid minus value for theta all the values are shifted $\pi/2$

$$\theta_{RangePoint} = \arctan \frac{Z_{iant} - Z_{RP}}{X_{iant} - X_{RP}} \quad (4.4)$$

Scattered field for each range point

Using (4.5) Scattered fields for each range point can be calculated. By definition it always happens when the antenna is in front of that pixel. It is clearly observed in Fig 4.6. r_{iRP} is the distance from this antenna to that special range point.

$$j_{ant} = \arg \min_{1 \leq i_{ant} \leq k} |x_{iant} - x_{iRP}| \quad (4.5)$$

In my implementation the value for σ_x is 10 and σ_θ is π . More details about σ_x , σ_θ can be found in [40]. Example of physical theta and optimal theta for the positions that object is presented is given in Fig 4.7 and Example of physical theta and optimal theta for the positions that artifact is presented is given in Fig 4.8.

It is clearly observed that in the positions that object is available the ratio of $\theta_{Physical}$ to $\theta_{Optimal}$ is close to one while for the places that artifact is present this ratio is close to zero.

After finding optimal theta and physical theta the ratio of amplitude from optimal theta to physical theta provide us a weighting function that will be later on added to SAR imaging formula (4.6).

$$I(m,n) = \sum_{k=1}^K \sigma \times S_k(t = T_{k,m,n}). \quad (4.6)$$

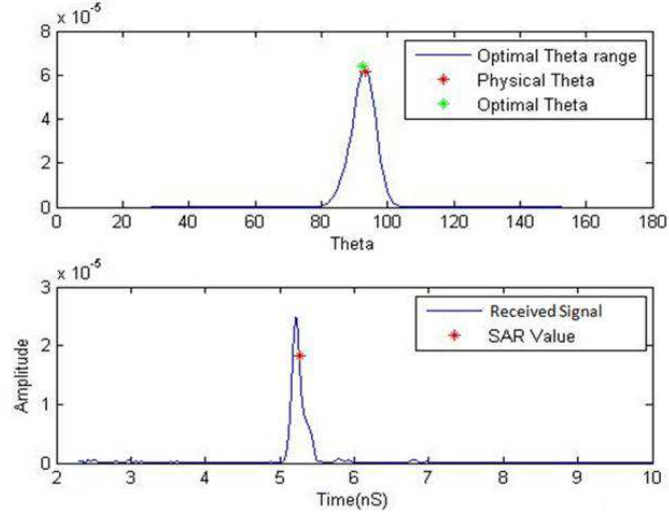


Figure 4.7: Antenna 35 for pixel (29,32) where the object is present.

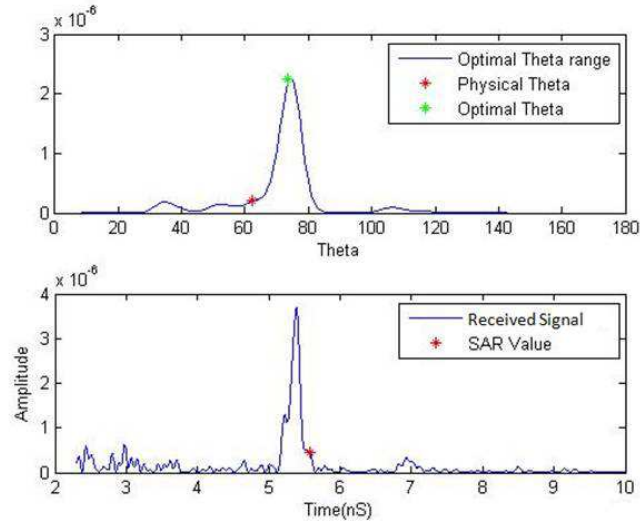


Figure 4.8: Antenna 25 for the position (26,49) where the artifact is happening

5

Result

In this chapter the SAR reconstructed image is presented for both rectangular metal plate and U shaped metal plate, the strong smile artefact around the object is clearly shown in these figures. The results of SAR imaging without artefact using another antenna behind the object and DOA method are also presented.

5.1 Readings from VNA and Preprocessing

In the first setup containing only one antenna working as both transmitter and receiver a rectangular metal plate is used as the object. The object is then moved along two separate paths one in red color $385mm$ from the antenna, see Fig 5.1 and the other a yellow path $715mm$ from the antenna, see Fig 5.2.

In Fig 5.1 the first column shows the raw data. The second column shows the subtraction of the raw data from the measurement without any object in front of the antenna. Theoretically this subtraction should remove the antenna's reflection, but as it is observed in Fig 5.1 and 5.2 second column we still have some reflection from the Antenna. In order to remove this reflection completely time gating can be used. The third column in fig Fig 5.1 and 5.2 shows the data after time gating. As it was explained earlier time gating will reject all readings exactly before the time in which antenna's reflection has been fully recorded. This time for all the measurements is $2.3nS$, which means all the recordings before this time are rejected so that antenna's reflection is removed, see Fig 5.1 and 5.2.

In Fig 5.1 and 5.2 a) shows the raw data in dB , b) is raw data in linear, c) and d) are the subtracted data in dB and linear respectively, figure e) and f) show the data in dB and linear after time gating respectively

It is important to note that in Fig 5.1 and 5.2 the first raw is in dB and the second raw is in liner scale.

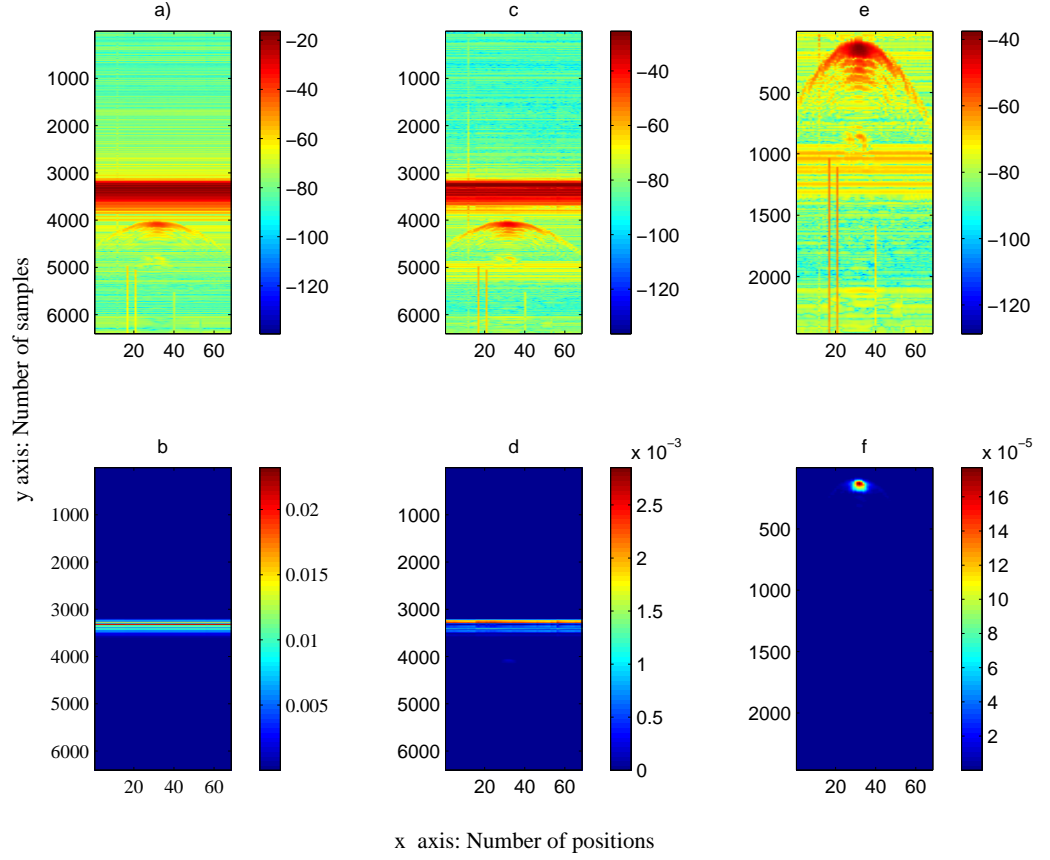


Figure 5.1: VNA recorded data for Red path

5.2 SAR Image from One Antenna

It was described in methods that we will reconstruct the final image using SAR algorithm (4.1). Results of SAR image from different objects moved in front of only one antenna along two paths (red and yellow) are given in this part.

5.2.1 SAR image reconstructed from one antenna and a rectangular metal plate

In Fig.5.3 and 5.4, SAR image of a rectangular metal plate moved along two paths of red and yellow is presented. Results are presented in both dB and linear scale. In Fig.5.3 and 5.4 object (the area with highest intensity) is the object. However it is clearly seen

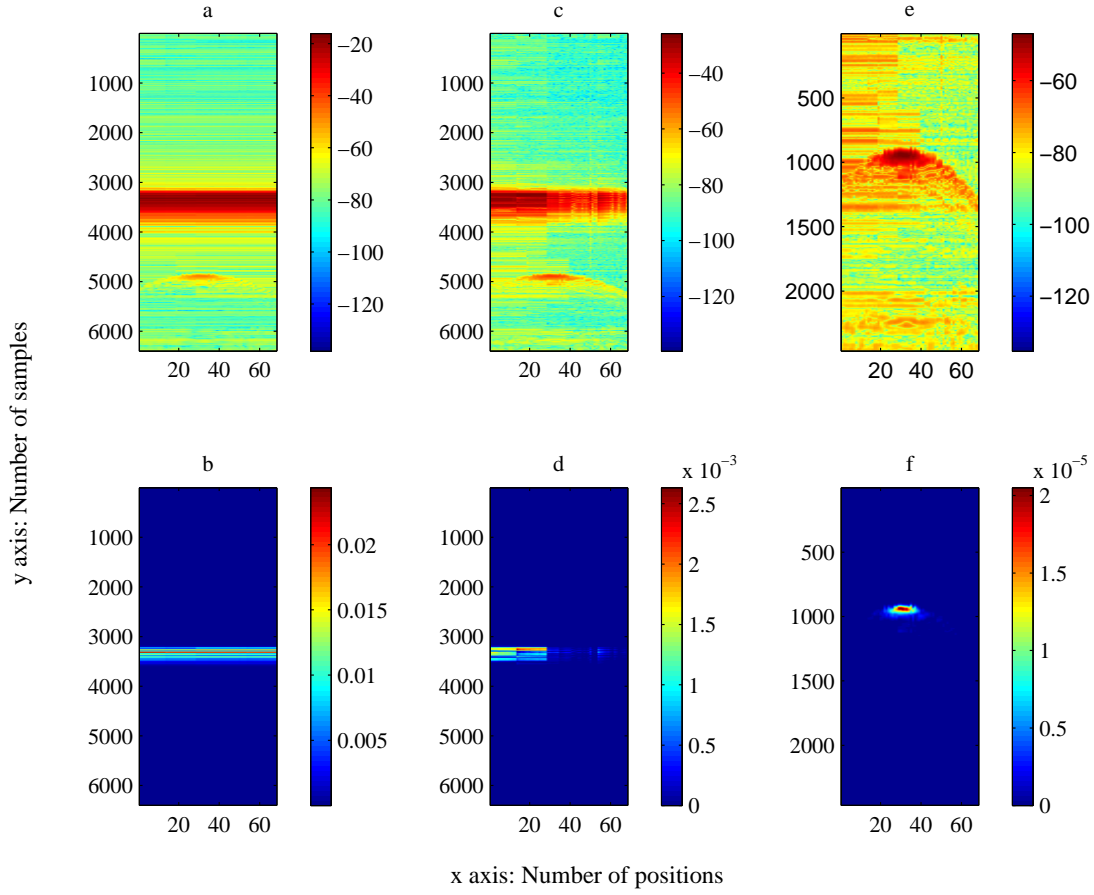


Figure 5.2: VNA recorded data for Yellow path

that object is buried in a smile shaped artifact originated from scattered fields of other antennas

In Fig5.3 figure a) and b) are reconstructed SAR image with resolution $16mm \times 10mm$ for red path in linear and dB respectively and figure c) and d) show the same but after normalization

In Fig5.5 figure a) and b) are reconstructed SAR image with resolution $16mm \times 10mm$ for yellow path in linear and dB respectively and figure c) and d) show the same but after normalization

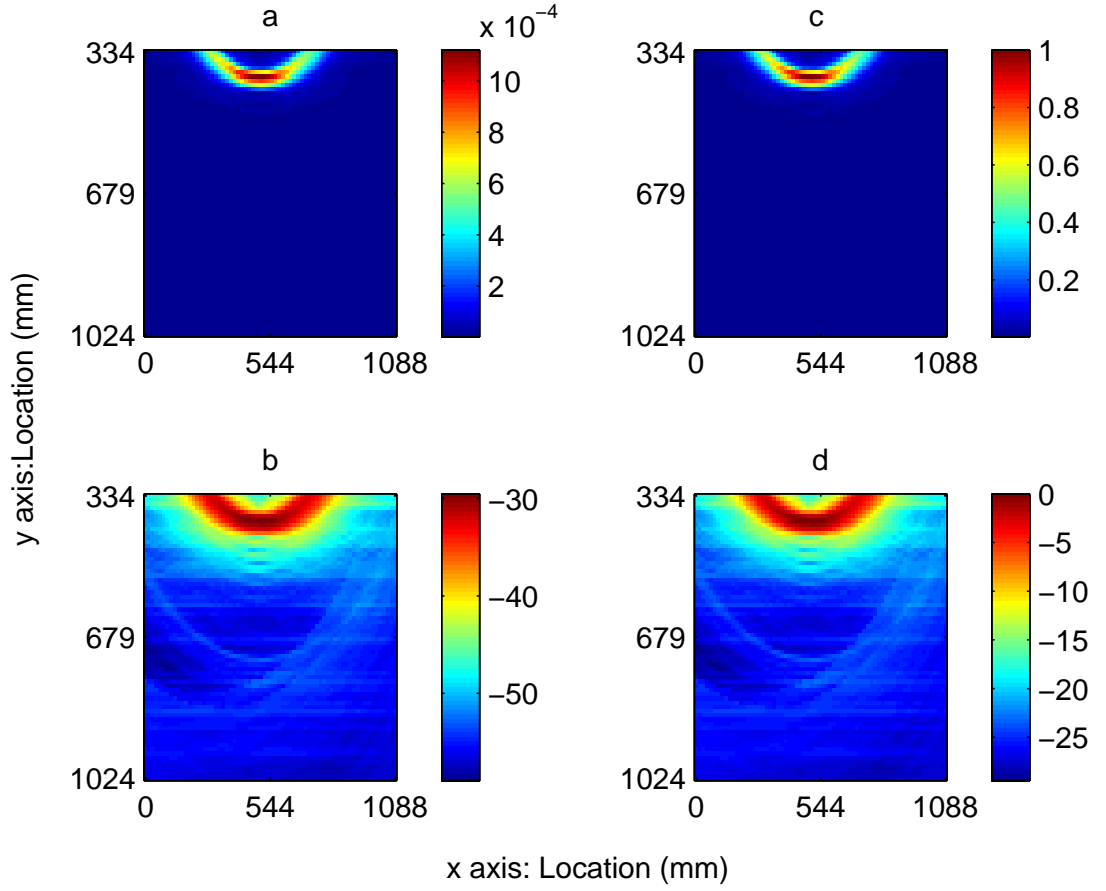


Figure 5.3: Reconstructed SAR image with resolution $16mm \times 10mm$ for red path

5.2.2 SAR image constructed from one antenna and a U shape metal plate

In the next step this rectangular metal plate is replaced by a *U* shaped metal plate. Results of SAR image for this new object are given in Fig.5.5.

In Fig.5.5 a) and b) are 1D reconstructed SAR image when the *U* shaped metal plate moves along red and yellow path respectively. Figure c) and d) are reconstructed SAR image when the object moves along red and yellow path and the antenna is behind the object so the Lego part comes first then the metal plate comes. The resolution of the entire figure is $16mm \times 10mm$.

In this set up we also rotate the object 180 degree so that the LEGO column holding the metal plate faces the antenna, results of the SAR image for this new situation is given in Fig.5.5 c) and d). LEGO column in middle of the metal plate can be seen in

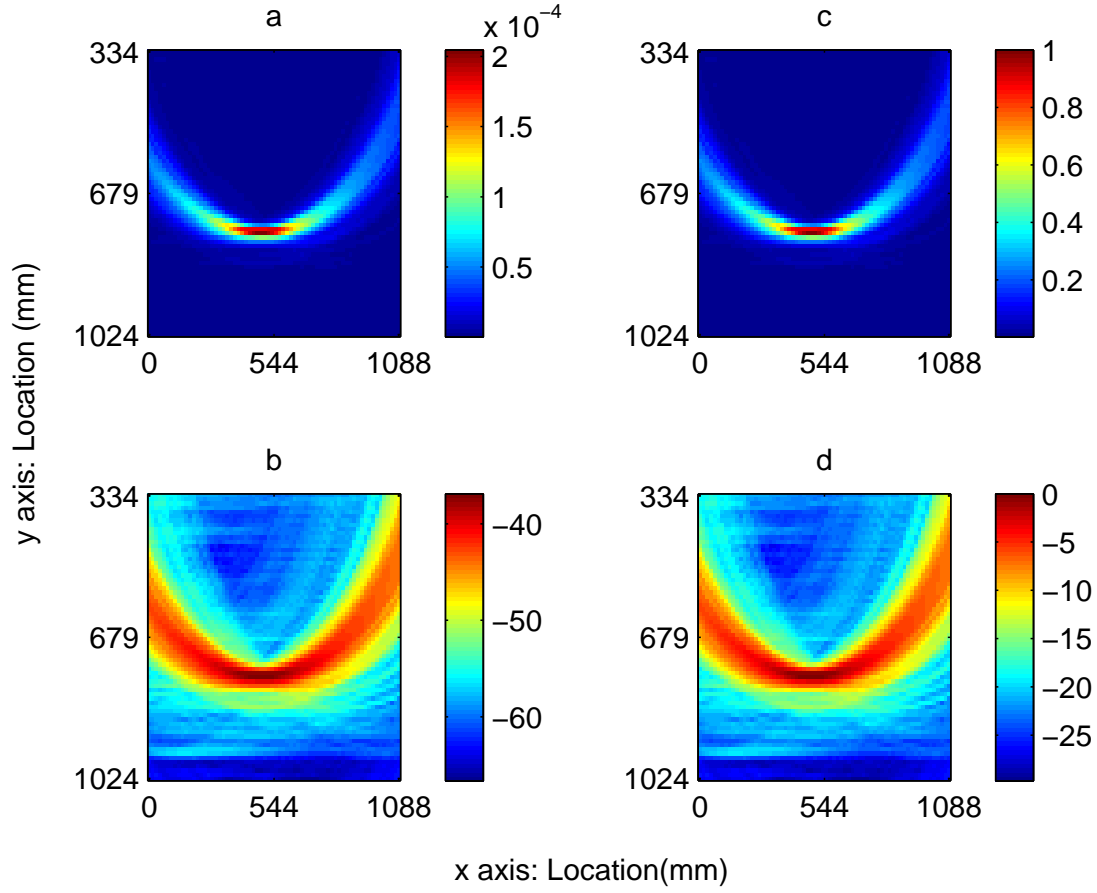


Figure 5.4: Reconstructed SAR image with resolution $16mm \times 10mm$ for yellow path

Fig.5.5.c) and d).

5.3 SAR Image from Two Antennas

In these section results of SAR image reconstructed in time domain in presence of two antennas is presented. In this mode one antenna will record scattered field data from behind the object and the other one will collect scattered fields in front of the object. Results of this setup are presented in this section when different objects are moved in the two red and yellow paths.

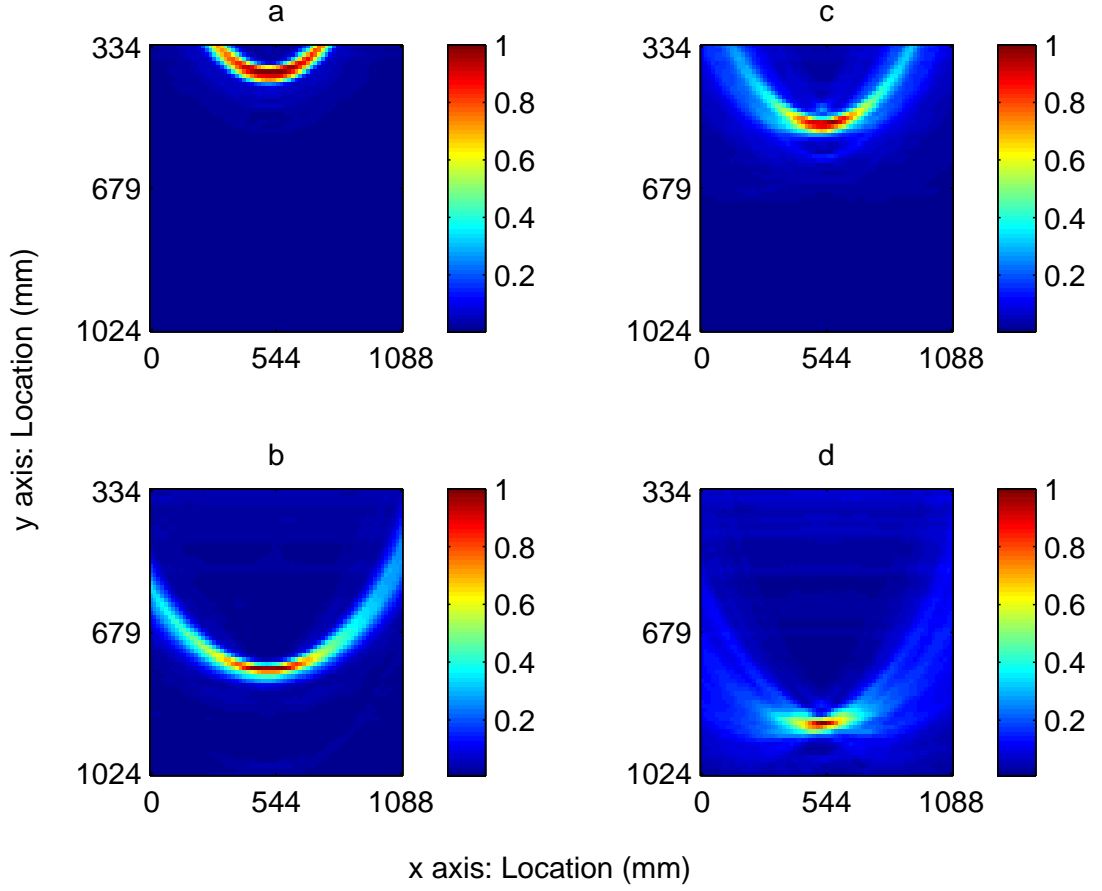


Figure 5.5: 1D reconstructed SAR image for U shaped metal plate

5.3.1 SAR image reconstructed from two antennas set up and a rectangular metal plate

As it was described earlier and already observed in Fig.5.3 and 5.4 there is a smile shaped artifact around the object in the final SAR image. One potential method to suppress this artifact is to measure scattered fields from behind the object and form another SAR image. This makes it essential to place another antenna behind the object recording scattered fields behind the object. Result of SAR image from scattered fields in front of the object is presented in Fig.5.6.a and Result of SAR image from scattered fields behind the object is presented in Fig.5.6.b. It is observed that in the SAR image from scattered fields behind the object the smile shaped artifact is 180 degree flipped changing from a smile to a cry.

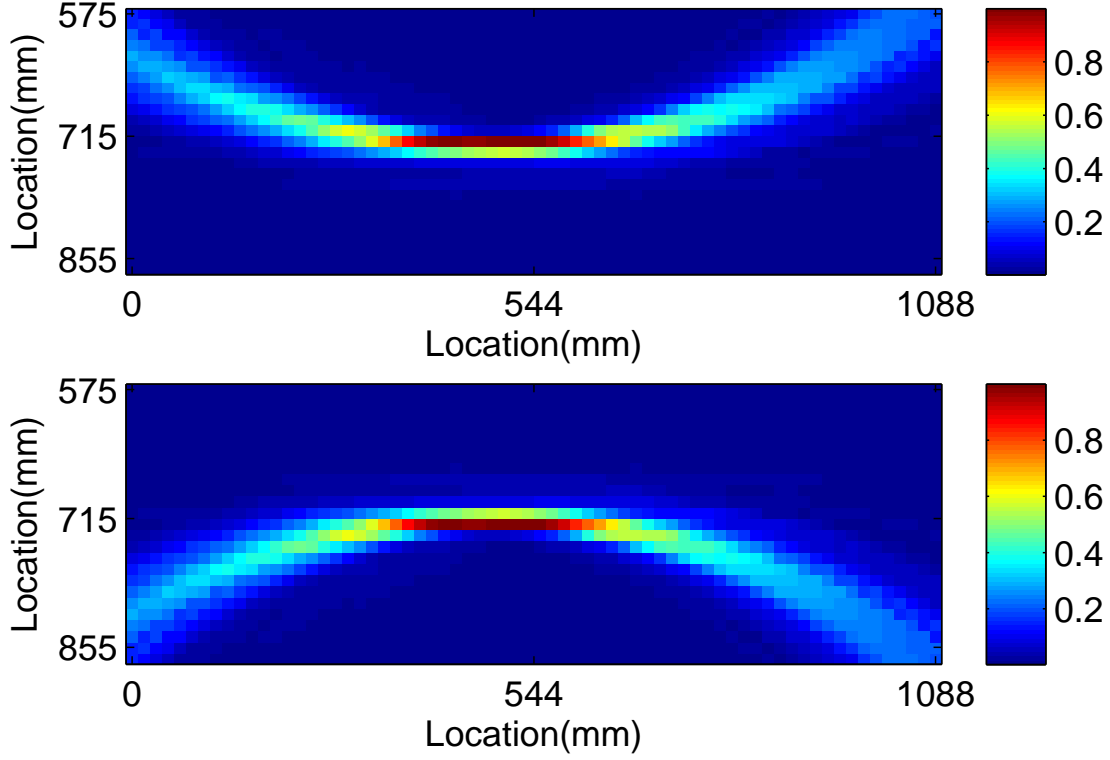


Figure 5.6: SAR image reconstruction results based on the front and back antenna

5.4 Artifact Rejection

As it was explained earlier and seen in all SAR images the final image of the object is always buried in a smile shaped artifact. In the SAR imaging algorithm at each position the distance the round-trip delay between the antenna and the pixel are calculated according to this distance. Then, the value of time domain signal at this calculated time is picked. If the object is present at this pixel, a strong signal is picked up and used for image reconstruction for this pixel. However, the same value is also picked up for other pixels with the same distance away from the same antenna position which is weaker. These weaker signals produce an artifact arc around the object.

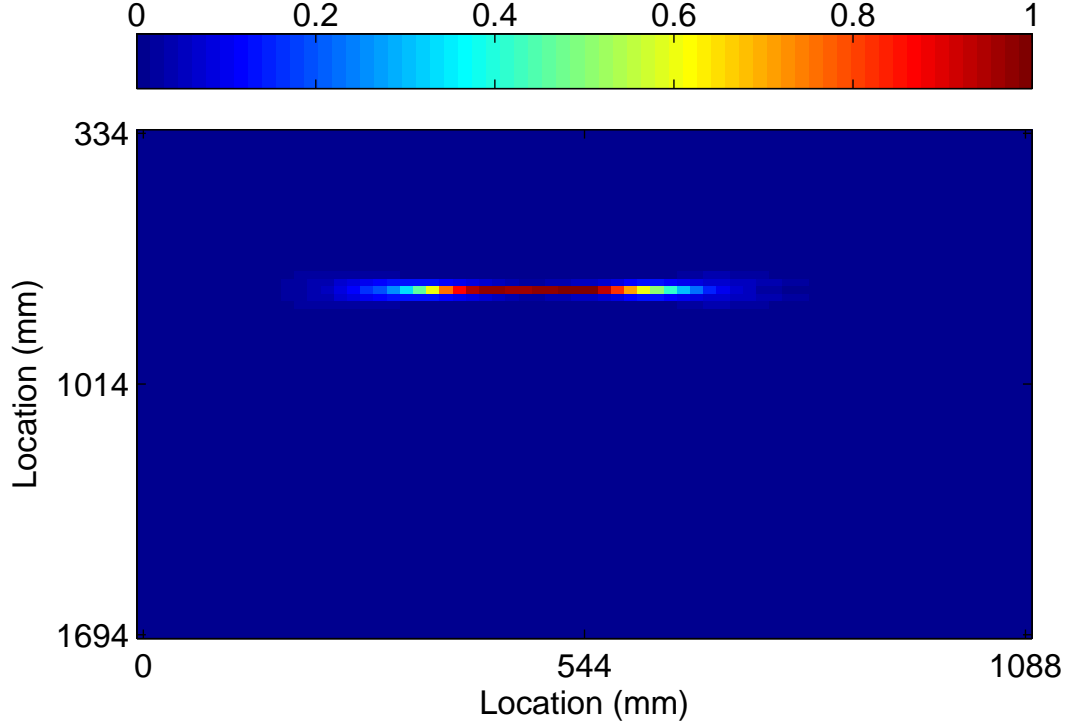


Figure 5.7: The resultant image after modified the algorithm

5.4.1 Artifact rejection using the scattered fields from behind the object

A very fast and easy method applicable to objects with a simple geometry is to record that from behind the object. This data will contain scattered fields from behind the object that are 180 degree rotated. These rotated scattered fields will produce a rotated version of image as well as the artifact associated with it, see Fig.5.6. Pixel by pixel multiplication these two images will enhance the quality of the objects image while canceling the artifact effect, see Fig.5.7.

5.4.2 Artifact rejection using directional of arrival (DOA) information

Since the recently proposed artifact rejection will not be applicable to objects with complex boundaries it is important to introduce an artifact rejection method that is fully functional in all situations and all object geometries. To do so the Range Point Migration (RPM) method can be used. This algorithm along with the global characteristics of the

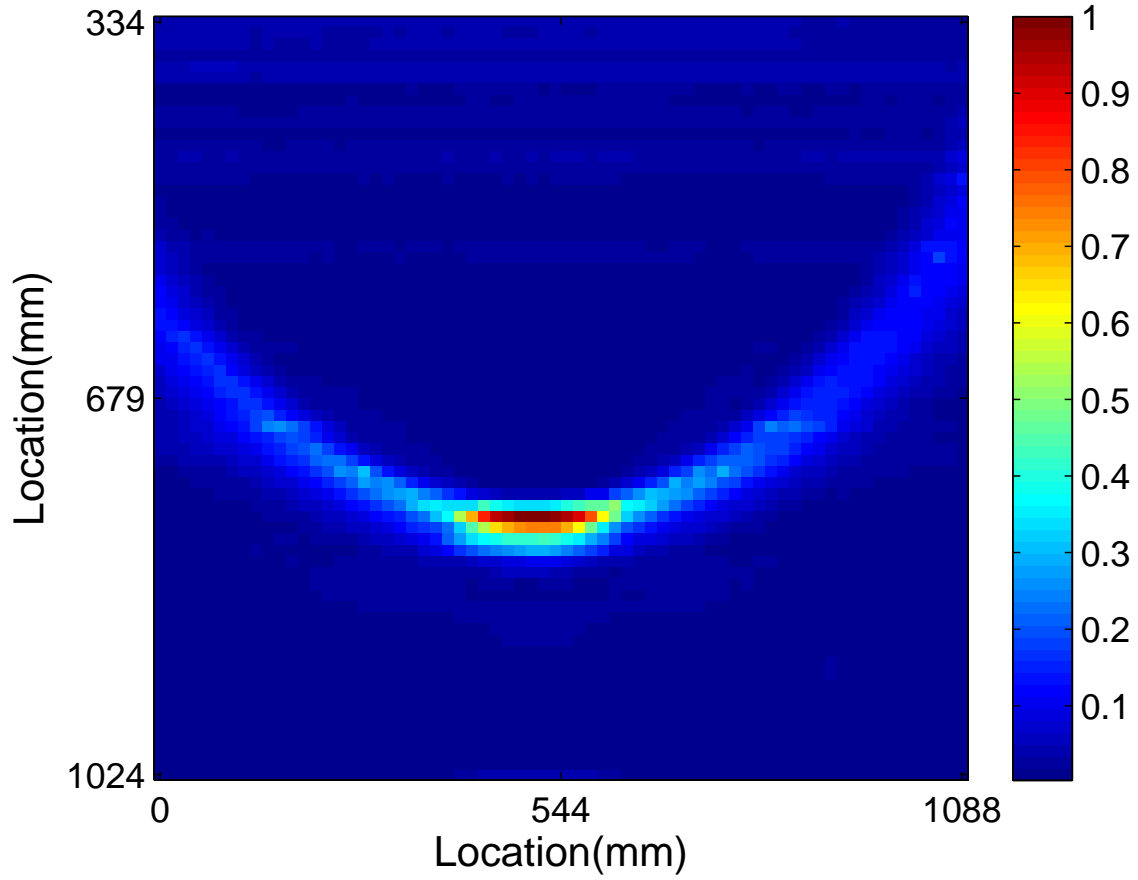


Figure 5.8: SAR reconstructed image after applying DOA method

observed range map can be used to calculate an optimum theta (θ_{opt}) for each antenna. This information along with the real physical direction of arrival at each position can produce a weighting factor that can be later on used to suppress undesired scattered fields producing the smile shaped artifact, see Fig.5.8. In Fig.5.8 object move along yellow path

However as it is observed in Fig.5.8 the smile shaped artifact is not fully suppressed and the final image of the object is thicker than the original object. This whole indicates that the DOA algorithm requires some preprocessing before being applied to the SAR algorithm. The very first step is to apply a threshold to the time domain data so that all the recordings but the main beam coming from the object is removed, see Fig.5.9

Now that we only have the main reflection from the object and all the other reflections are set to zero, we perform a scan over each column and using the distance between the antenna and each pixel we will calculate the time in which the value of VNA signal should be picked, see Fig.5.10

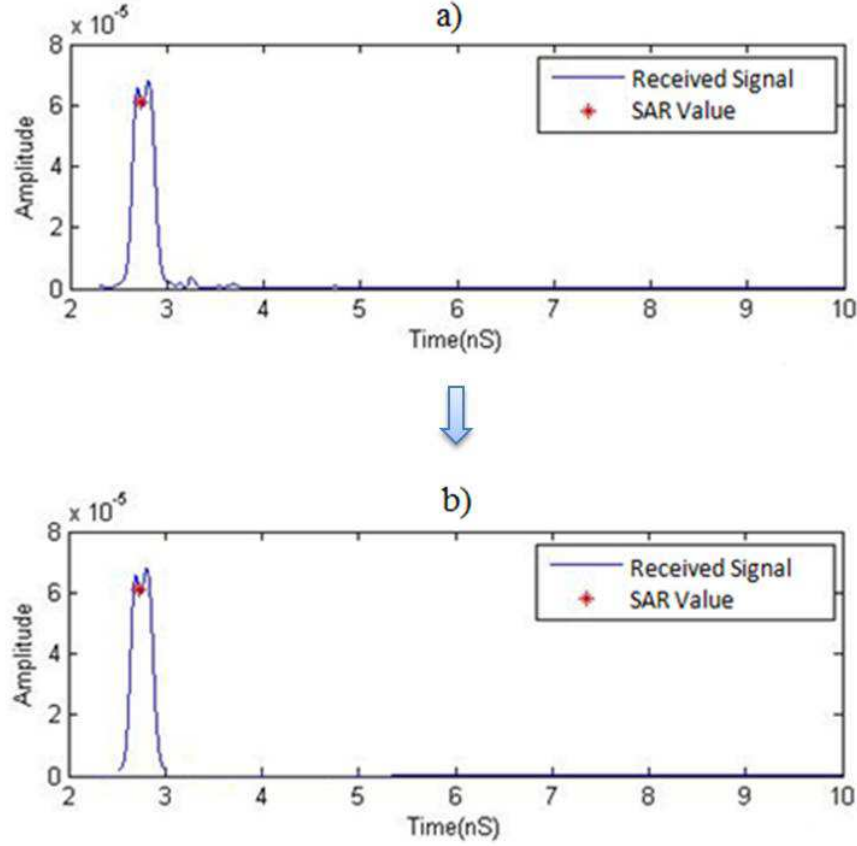


Figure 5.9: a) Received signal with SAR value and b) The noise is removed

Since all the values of VNA signal except the main beam (coming from the object) are set to zero, if the picked value is zero we conclude there is no object at that pixel see Fig.5.11, while if there is a none zero value we conclude that the object is present at that pixel, see Fig.5.12.

Using this fast and simple scan we determine the location of the object. Using this information at each pixel if the object is presented we calculate the SAR value for that pixel and then apply the DOA weighting factor to it, otherwise we set the value of SAR for that pixel to zero. In this way the scattered fields in the locations that object is not presented is set to zero very fast, and using the DOA weighting factor the effect of adjacent attends at that pixels where the object is presented is tuned according to the weighting factor. This whole will lead to the suppression of the final SAR image artifact, see Fig.5.13.

Although in Fig.5.13 the artifact is very well suppressed we still see that the final image is thicker than the original object. To overcome this issue we need to have a closer look at each column. To do so we will plot all the values that are picked along one column on a single time domain recording from VNA, see Fig.5.14. It is observed that despite

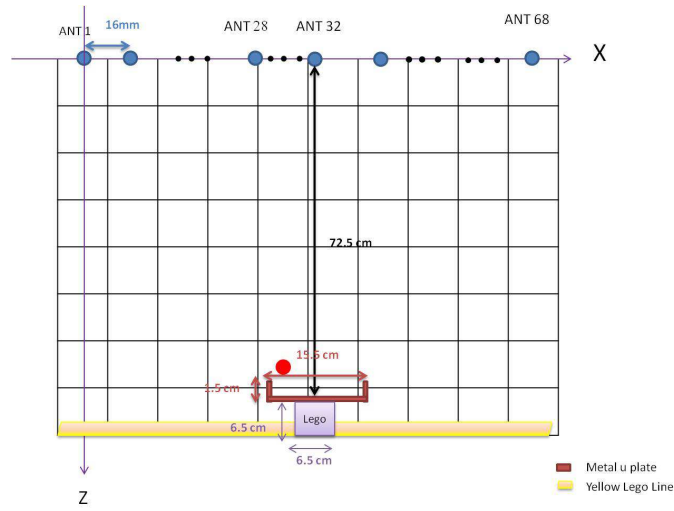


Figure 5.10: Real geometry of *U* shaped metal object in yellow path when antenna is in front of the object

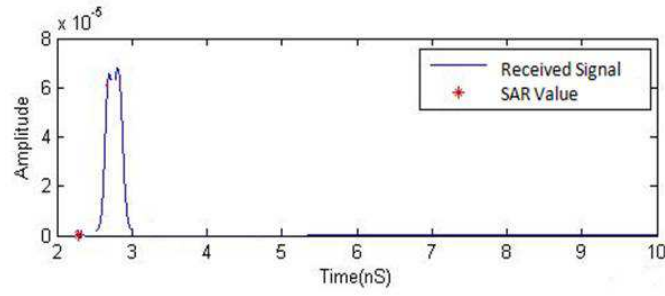


Figure 5.11: The picked value is zero

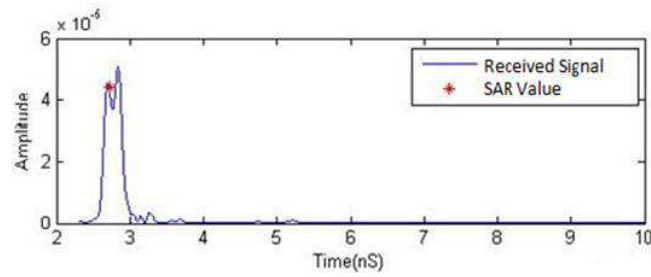


Figure 5.12: The picked value is non zero

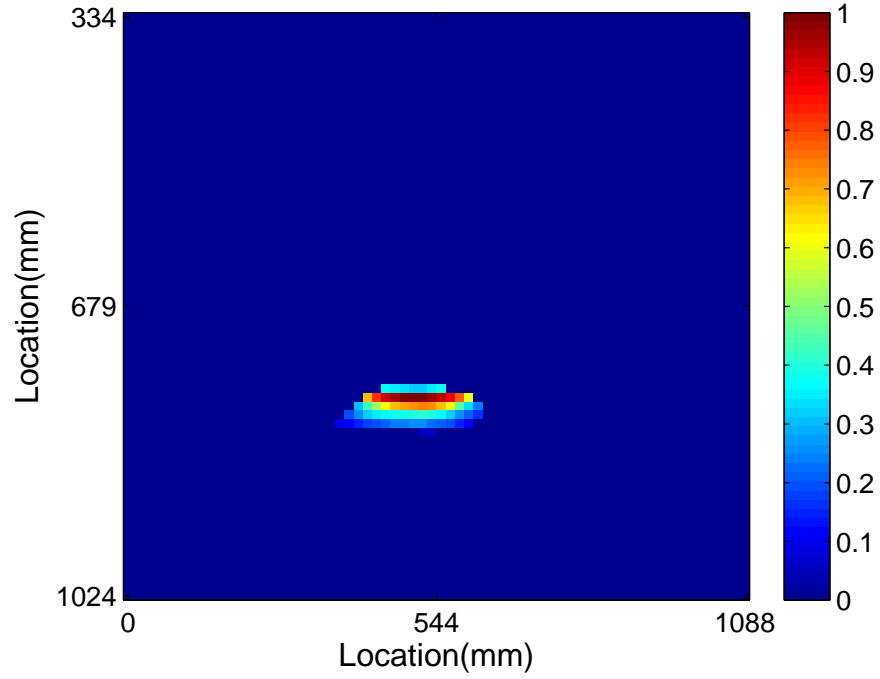


Figure 5.13: Reconstructed SAR image after applying Threshold and scanning the pixels

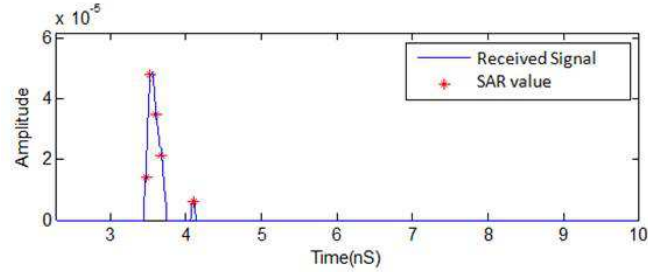


Figure 5.14: Five pixels in the column in front of one antenna where the object is present are picked

our expectation that there should only exist one pixel (position that object is present) with none zero value, some other positions are also picked (most probably pixels that are very close to the object). One hypothesis to this could be the wide bandwidth of the time domain signal. To narrow the bandwidth we can use the first derivative of the time domain signal, see Fig.5.15. Using this narrowed signal we will have fewer positions for reconstruction purpose and the final image will be free of artifact with the same width as the original object, see Fig.5.16

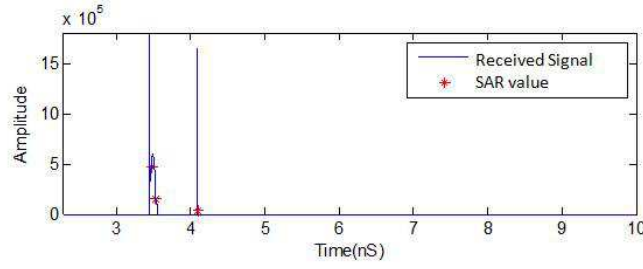


Figure 5.15: Three pixels in the column in front of one antenna where the object is present are picked

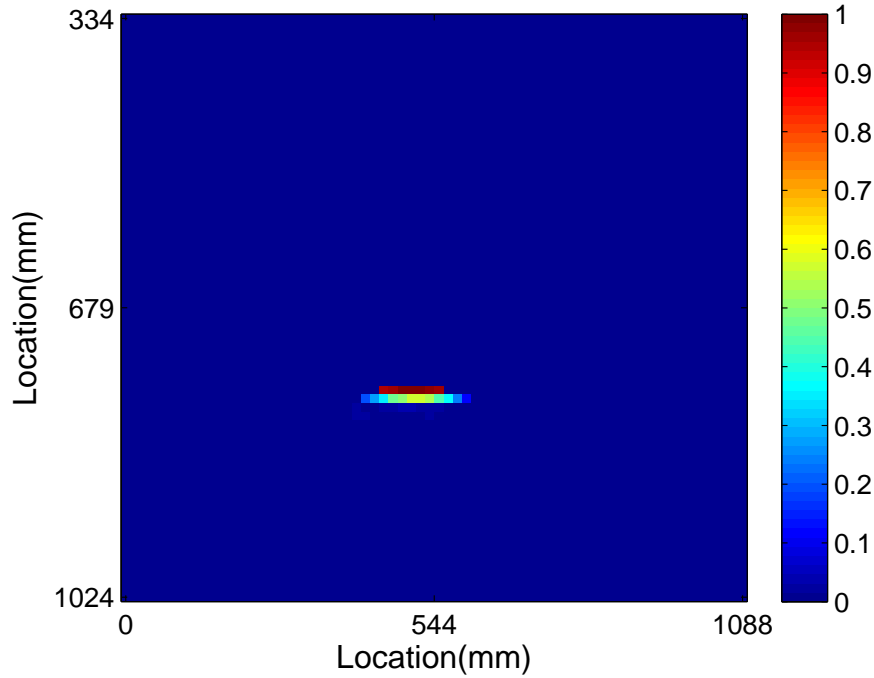


Figure 5.16: SAR reconstructed final image

The algorithm is also verified by simulated data using FEKO. In this simulation, totally there are 68 sensors located along the x direction within $1m$. $d_x = 1/(68 - 1) = 0.0149m$. For each valuable, it is a $68 \times 68 \times 256$ matrix. 68×68 corresponds to the transmit and receive combination. 265 correspond to the sample in time. The maximum excitation frequency is $13.5GHz$. For matching the time with measured data the interpolation method is applied and the results are shown in Fig.5.17. In this simulation the time domain data is the Electric field (V/m). The time domain data from VNA is the power signal. In order to have the same as the VNA data, we take the square of each

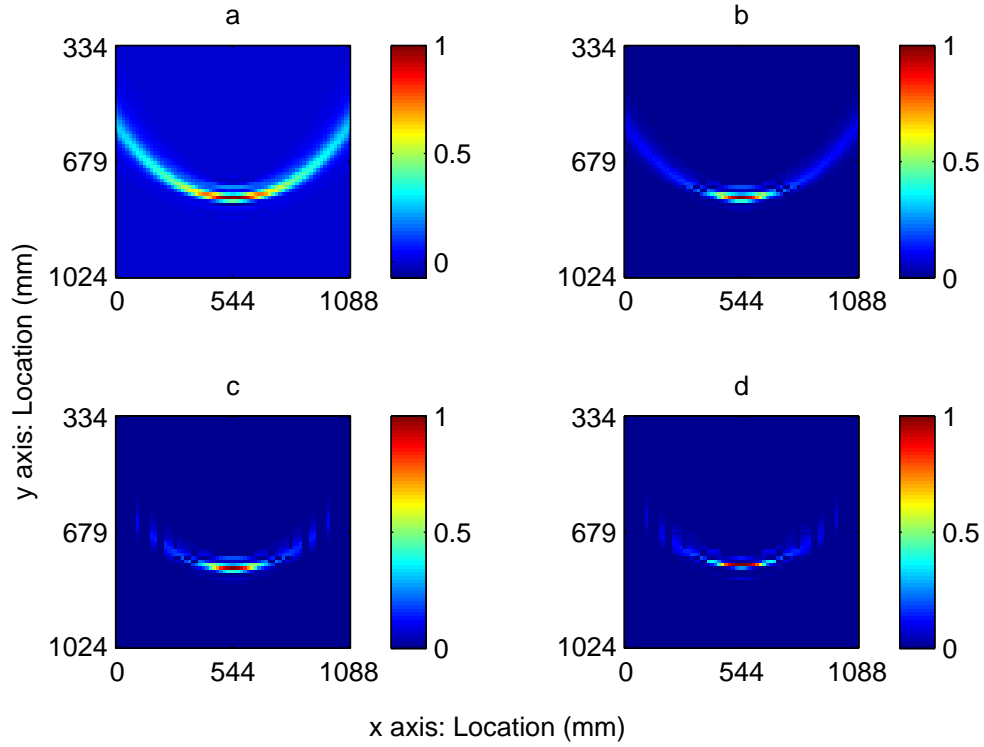


Figure 5.17: SAR reconstructed image from simulated data

sample before doing the image reconstruction

The results of SAR imaging is shown in Fig.5.17.a) as it is obvious there is strong artefact around the object. In fig b) this artefact is reduced using RPM then in fig c) the scan over the entire pixel is applied and finally we get the derivative of antenna signals and the result is shown in the last figure.

6

Conclusions and Future Work

6.1 Discussion

Near field imaging of objects using Ultra Wide band UWB and Synthetic Aperture Radar SAR imaging can be achieved using scattered fields received from the object. In this thesis work we were able to propose a simple setup for SAR imaging algorithm, implement the algorithm and show one of its main weak points that is the artifact from scattered fields of adjacent antennas. Since the SAR algorithm uses the same value of all scattered fields received at each pixel the quality of the final image is highly decreased. An extensive study was performed to understand the sources of this artifact in SAR final image and finally two methods were proposed to suppress this artifact. However the main object used in this thesis work is mainly a metal plate with high reflective properties. Great attention has been paid to UWB operating in synthetic aperture mode (SAR) for detection of metal objects like mines and unexploded ordnance buried in the soil that are rather large metallic objects [2], [10],[41], [42]. The resolution of the imaging technique has been highly improved so that even similar objects like exploded and unexploded mines can be distinguished. But not many studies have been performed to the objects with smaller size and different dielectric properties like foreign object within the food. Now that the measurement protocols, functional set up and sources of artifact are recognized and enhanced, it is of great value to first study the ability of SAR imaging algorithm for imaging of materials with different dielectric properties like food and then study the resolution of the SAR for classifying different material within an object like pieces of plastic or stone in food.

6.2 Conclusion

A modified UWB-SAR algorithm is presented for imaging of object in the near field region. It has been shown by measurement that although the algorithm is able to produce an image of the object the quality of the final image is very much decreased by the presence of undesired scattered fields from adjacent objects. These scattered fields will produce "smile" shape artefacts. A very simple and fast method to suppress this artifact is presented. This method suggests that using another antenna behind the object and recording the scattered fields behind the object, it is possible to produce a mirrored version of object's image in which the artifact is also mirrored. Therefore pixel by pixel multiplications of these two images will cancel the artifact. Since this method is not applicable to objects with complex geometry and boundaries, another method based on the information of direction of arrival of (DOA) of scattered fields at each pixel was introduced. Both these methods were tested and their feasibility was shown on SAR images obtained from real measurements

6.3 Future Work

Now that the modified UWB-SAR imaging algorithm proposed in this paper is fully tested and enhanced in terms of artifact rejection, it is important to test this method for different objects with different dielectric properties like food. Later on it is important to enhance the measurement set up and increases the number of antennas from two antennas to at least ten antennas and increases the resolution of the final image. Right now an array of antennas consisting of ten Bow-Tie antennas is produced and ready to use for UWB-SAR imaging algorithm. We aim to replace the metal object with small piece of food and test the ability of our proposed UWB-SAR algorithm in detection of foreign objects within the food.

Bibliography

- [1] Food Radar System AB. “<http://www.foodradar.com/>”.
- [2] Y. Wang, I. D. Longstaff, C. J. Leat, “SAR Imaging of Buried Objects from MoM modelled scattered field”, *IEE Proc Radar Sonar and Navigation*, vol. 148, no. 3, pp. 167–172, 2001.
- [3] J. Yang, A. Kishk, “A novel low-profile compact directional ultrawideband antenna: the self-grounded Bow-Tie antenna”, *IEEE Trans Antennas Propagat*, vol. 60, no.3, pp. 1214–1220, 2012.
- [4] J. Yang, A. Kishk, “The self-grounded Bow-Tie antenna”, *IEEE AP-S International Symp on Antennas Propag*, 3-8 July, Spokane Washington, 2011.
- [5] Antenna Engineering Laboratory exercise 2 “Measurments of radiation pattern and gain for antennas in line-of-sight environment in anechoic chamber at chalmers university”.
- [6] D. Kim, S. Shin, “Experiments for Ultra-Wideband Imaging Radar with One-Dimensional Synthetic Aperture”, *Synthetic Aperture Radar (AP SAR), 3rd International Asia-Pacific*, Page(s) 1- 4, 2011.
- [7] J. D. Taylor, *Ultra-wideband Radar System*, CRC press, 1995.
- [8] U. S. C, Viterbi School of Engineering, Archived from the original 2012-03-21.
- [9] S. S. Fayazi, H. S. Lui, J. Yang, “Microwave Imaging of Near-Field Object Using Ultra-Wideband Synthetic Aperture Radar Algorithm”, *2012 IEEE Antennas and Propagation Society International Symposium*, Chicago, 2012.
- [10] S. Vitebskiy, L. Carin, M. A. Ressler, F. H. Le, “Ultra-Wideband Short-Pulse Ground-Penetrating Radar Simulation and Measurement”, *IEEE Trans Geoscience and Remote Sensing*, vol. 33, no. 3, pp. 762–772, 1997.

- [11] H. S. Lui, N. V. Z. Shuley, "Radar Target Recognition using a Banded E-Pulse Technique", *IEEE Trans Antennas and Propagation*, vol. 54, no. 12, pp. 3874-3881, 2006.
- [12] R. Olsson, P.-S. Kildal, S. Weinreb, "The Eleven antenna: a compact low-profile decade bandwidth dual polarized feed for reflector antennas", *IEEE Transactions on Antennas and Propagation*, vol. 54, no. 2, pp. 368-375, 2006.
- [13] P.-S. Kildal, R. Olsson, J. Yang, "Development of three models of the Eleven antenna: a new decade bandwidth high performance feed for reflectors", in: *First European Conference on Antennas and Propagation (EuCAP 2006)*, 2006, pp. 1-6.
- [14] J. Yang, X. Chen, N. Wadefalk, P.-S. Kildal, "Design and realization of a linearly polarized Eleven feed for 1-10 GHz", *IEEE Antennas and Wireless Propagation Letters*, vol. 8, pp. 64-68, 2009.
- [15] J. Yang, D. Nyberg, J. Yin, "Impedance matrix of a folded dipole pair under Eleven configuration", *IET Microwaves, Antennas & Propagation*, vol. 4, no. 6, pp. 697-703, 2010.
- [16] J. Yang, "On conditions for constant radiation characteristics for log-periodic array antennas", *IEEE Transactions on Antennas and Propagation*, vol. 58, no. 5, pp. 1521-1526, 2010.
- [17] J. Yang, P.-S. Kildal, "Optimization of reflection coefficient of large log-periodic array by computing only a small part of it", *IEEE Transactions on Antennas and Propagation*, vol. 59, no. 6, pp. 1790-1797, 2011.
- [18] J. Yang, M. Pantaleev, P.-S. Kildal, B. Klein, Y. Karandikar, L. Helldner, N. Wadefalk, C. Beaudoin, "Cryogenic 2-13 GHz eleven feed for reflector antennas in future wideband radio telescopes", *IEEE Transactions on Antennas and Propagation*, vol. 59, no. 6, pp. 1918-1934, 2011.
- [19] J. Yang, M. Pantaleev, P. Kildal, L. Helldner, "Design of compact dual-polarized 1.2-10 GHz Eleven feed for decade bandwidth radio telescopes", *IEEE Transactions on Antennas and Propagation*, vol. 60, no. 5, pp. 2210-2218, 2012.
- [20] H. Raza, J. Yang, A. Hussain, "Measurement of radiation efficiency of multiport antennas with feeding network corrections", *IEEE Antennas and Wireless Propagation Letters*, vol. 11, pp. 89-92, 2012.
- [21] J. Yin, J. Yang, M. Pantaleev, L. Helldner, "The circular Eleven antenna: a new decade-bandwidth feed for reflector antennas with a high aperture efficiency", *IEEE Transactions on Antennas and Propagation*, no. 61, 2013.
- [22] X. Chen, P. Kildal, J. Carlsson, J. Yang, "Comparison of ergodic capacities from wideband MIMO antenna measurements in reverberation chamber and anechoic

- chamber”, *IEEE Antennas and Wireless Propagation Letters*, vol. 10, pp. 446–449, 2011.
- [23] X. Chen, P.-S. Kildal, J. Carlsson, J. Yang, “MRC Diversity and MIMO Capacity Evaluations of Multi-Port Antennas Using Reverberation Chamber and Anechoic Chamber”, *IEEE Transactions on Antennas and Propagation*, vol. 61, 2013.
- [24] J. Yin, J. A. Aas, J. Yang, P.-S. Kildal, “Monopulse tracking performance of multi-port eleven antenna for use in satellite communications terminals”, in: *The Second European Conference on Antennas and Propagation, 2007. EuCAP 2007*.
- [25] R. Wang, J. Yang, “A new compact antenna for digital television reception based on the eleven antenna”, *Microwave and Optical Technology Letters*, vol.53, no. 4, pp. 824–827, 2011.
- [26] A. Yasin, J. Yang, T. Ostling, “A compact dual-band feed for reflector antennas based on choke horn and circular Eleven antenna”, *IEEE Transactions on Antennas and Propagation*, vol. 57, no. 10, pp. 3300–3302, 2009.
- [27] S. Abtahi, J. Yang, S. Kidborg, “A new compact multiband antenna for stroke diagnosis system over 0.5–3 GHz”, *Microwave and Optical Technology Letters*, vol. 54, no. 10, pp. 2342–2346, 2012.
- [28] Y. Yu, J. Yang, T. McKelvey, B. Stoew, “A Compact UWB Indoor and Through-Wall Radar with Precise Ranging and Tracking”, *International Journal of Antennas and Propagation* 2012.
- [29] P. Kildal, J. Yang, “FDTD optimizations of the bandwidth of the hat feed for MM-wave reflector antennas”, in: *1997 IEEE Antennas and Propagation Society International Symposium*, vol.3, pp. 1638–1641, 1997, IEEE, 1997.
- [30] J. Yang, P. Kildal, “Gaussian vertex plate improves return loss and far-out sidelobes in prime-focus reflector antennas”, *Microwave and Optical Technology Letters*, vol. 21, no. 2, pp. 125–129, 1999.
- [31] J. Yang, P. Kildal, “Calculation of ring-shaped phase centers of feeds for ring-focus paraboloids”, *IEEE Transactions on Antennas and Propagation*, vol. 48, no. 4, pp. 524–528, 2000.
- [32] M. Denstedt, T. Ostling, J. Yang, P. Kildal, “Tripling bandwidth of hat feed by genetic algorithm optimization”, in: *2007 IEEE Antennas and Propagation Society International Symposium*, IEEE, 2007, pp. 2197–2200.
- [33] W. Wei, J. Yang, T. Ostling, T. Schafer, “New hat feed for reflector antennas realised without dielectrics for reducing manufacturing cost and improving reflection coefficient”, *IET Microwaves, Antennas & Propagation*, vol. 5, no.7, pp. 837–843, 2011.

- [34] E. G. Geterud, J. Yang, T. Ostling, P. Bergmark, "Design and optimization of a compact wideband hat-fed reflector antenna for satellite communications", *IEEE Transactions on Antennas and Propagation*, vol. 61, no. 1, 2013.
- [35] J. Yang, U. Carlberg, P. Kildal, M. Kehn, "A fast mode analysis for waveguides of arbitrary cross section with multiple regions by using a spectrum of two-dimensional solutions and asymptotic waveform evaluation", *IEEE Transactions on Microwave Theory and Techniques*, vol.52,no.6, pp. 1615-1621, 2004.
- [36] J. Yang, U. Carlberg, P. Kildal, M. Kehn, "A fast mode analysis for waveguides of arbitrary cross section with multiple regions by using a spectrum of two-dimensional solutions and asymptotic waveform evaluation", *IEEE Transactions on Microwave Theory and Techniques*, vol. 52, no. 6, pp. 1615–1621, 2004.
- [37] J. Yang, P. Kildal, "Presentation of the spectral electric and magnetic field integral equations used in G2DMULT for analyzing cylindrical structures of multimaterial regions", *Microwave and Optical Technology Letters*, vol.34, no.2, pp. 88–93, 2002.
- [38] Agilent Time Domain Analysis Using a Network Analyzer Application Note 1287-12.
- [39] S. Kidera, T. Sakamoto, T. Sato, "Super-Resolution UWB Radar Imaging Algorithm Based on Extended Capon With Reference Signal Optimization".
- [40] S. Kidera, T. Sakamoto, T. Sato, "Accurate UWB radar 3-D imaging algorithm for complex boundary without range points connections", *IEEE Trans Geosci Remote Sens*, vol. 48, no. 4, pp. 1993-2004, 2010, 2010.
- [41] L. Carlin, N. Geng, M. McClure, J. Sichina, L. Nguyen, "Ultra-wide-band synthetic aperture radar for min-field detection", *IEEE Trans Antennas Propaga MAG*, vol. 41, no. 1, pp. 18-32, 1991.
- [42] C. Chen, L. Peters, "unexploded ordnance identification via complex natural resonances", *IEEE Trans Antennas Propag*, vol. 45, no.2, pp. 1645-1654, 1997.

A

List Of Publications

A.1 Paper A

Microwave Imaging of Near-Field Object Using Ultra-Wideband Synthetic Aperture Radar Algorithm

Seyedeh Shaghayegh Fayazi, Hoi-Shun Lui and Jian Yang

Paper presented at the IEEE International Symposium on Antennas and
Propagation AP-S and USNC-URSI National Radio Science meeting. Chicago,
USA, July 8-14, 2012.

Microwave Imaging of Near-Field Object Using Ultra-Wideband Synthetic Aperture Radar Algorithm

Seyedeh Shaghayegh Fayazi

Dept. of Applied Physics and Electronics
Umea University of Technology, Umea, Sweden
Dept. of Signals and Systems
Chalmers University of Technology, Gothenburg, Sweden
fayazi@student.chalmers.se

Hoi-Shun Lui and Jian Yang

Dept. of Signals and Systems
Chalmers University of Technology
Gothenburg, Sweden
antony.lui@chalmers.se
jian.yang@chalmers.se

Abstract—A simple procedure that suppresses artefact from ultra-wideband (UWB) synthetic aperture radar (SAR) images is proposed and verified using experimental data. The proposed imaging solution is useful for imaging small objects located in the near-field region with less ambiguity.

I. INTRODUCTION

Ultra-wideband (UWB) technology and its use in imaging and sensing have drawn significant interest in the last two decades. Extensive studies have contributed to utilizing UWB transient scattering for automated target recognition [1] and imaging purposes [2], [3]. In [2] and [3], a UWB synthetic aperture radar (SAR) imaging algorithm was presented and applied for subsurface object imaging. One limitation of the algorithm is that an artefact in the imaging procedure causes ambiguity. In this work, a simple modified procedure is proposed to reduce such artefact. The feasibility of the proposed algorithm is presented and verified using experimental data.

II. EXPERIMENTAL SETUP

The UWB imaging system for objects in near-field region is shown in Fig.1. It consists of a self-grounded Bow-Tie antenna [4], [5] located in front of the object, a vertically-placed rectangular metal plate. To obtain multiple views, the metal plate is placed in 68 equal-spaced positions along a straight line of 1088 mm long, and the monostatic responses at each of these 68 positions are measured using a network vector analyzer (VNA) from 0.5 GHz to 13 GHz. The above setup is equivalent to the case that a single antenna moves along a straight line in front of the static object, and transmits and receives the monostatic responses at these 68 positions, as shown in Fig. 2. Therefore, the SAR algorithm can be employed to have an imaging of the object.

In order to have a high flexible and accurate positioning system for the measurement at a low cost in this study, a straight path of 1088 mm long was built up of 68 Duplos LEGO blocks, shown in Fig.1. Each Duplos block has a length of 16 mm, and the distance between the antenna and the LEGO path is 715 mm. The entire measurement is performed

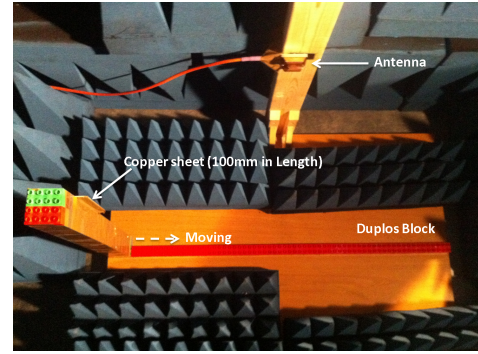


Fig. 1. Experimental setup.

in an anechoic chamber in this preliminary study, so that the reflections from surroundings are minimized. We have developed an algorithm to suppress the reflections from indoor environment and will soon apply it into this imaging project.

The monostatic responses in time domain, which is used for image reconstruction, are obtained via an Inverse Fourier Transform of the frequency samples provided by the VNA measurement.

III. IMAGING ALGORITHM PRINCIPLE

An object with a simple geometry, a metal sheet with a length of 100 mm, is considered for the imaging, shown in Fig. 1. When the object is placed at the 68 position, it is equivalent to that the object is located in front of an array of 68 antenna elements, shown in Fig. 2. This setup is similar to those described in [2], [3], except for that only the monostatic responses are measured and used here. The intensity of each pixel $I(m, n)$ is given by

$$I(m, n) = \sum_{k=1}^K S_k(t = T_{k, m, n}). \quad (1)$$

where S_k is the received signal of antenna k , and $T_{k, m, n}$ is the round-trip time delay between the k th antenna and the

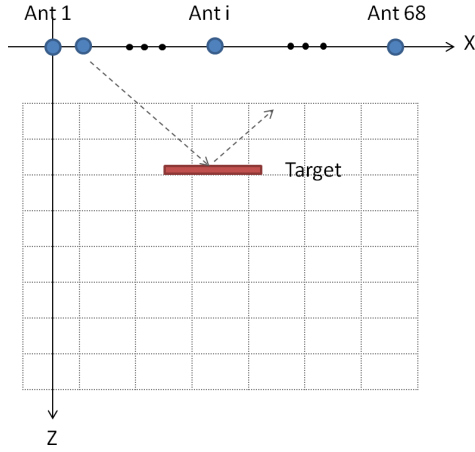


Fig. 2. The geometry of the SAR configuration.

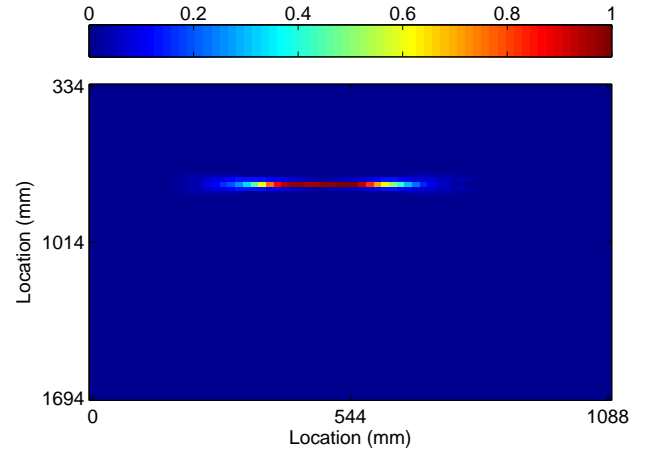


Fig. 4. The resultant image after modified algorithm

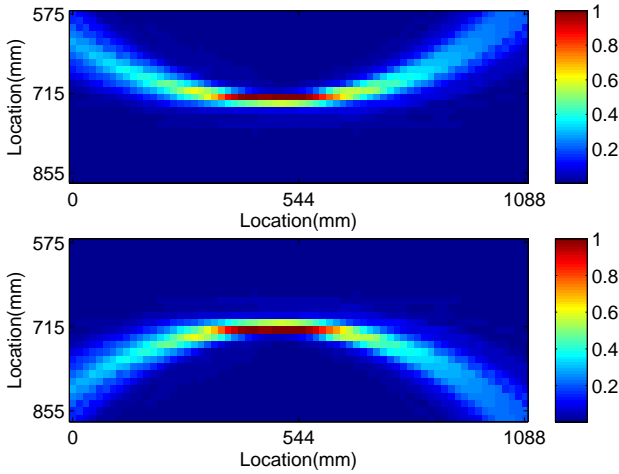


Fig. 3. Image reconstruction results based on: (a) the front antenna (up); (b) the back antenna (down)

physical position of the pixel (m, n) .

IV. MODIFIED ALGORITHM AND RESULTS

The image is reconstructed by using (1) and shown in Fig. 3 (up). The vertically-placed metal plate is observed but it comes with a “smile” shape around it. This smiling is an undesirable artefact introduced from the algorithm. The reason is discussed as follows.

When the image is constructed, the distance d and the round-trip delay $t_d = 2d/c$ between the antenna and the pixel are calculated. Then, the signal $S(t = t_d)$ is chosen. If the object is present at this pixel, a strong signal $S(t = t_d)$ is picked up and used for image reconstruction for this pixel. However, the same value is also picked up for other pixels with the same distance d away from the same antenna position. Thus, an artefact arc is formed. In this work, a simple metallic plate is used and the arc forms a “smile” in the resultant image.

To remove this artefact, we use the same antenna moving in the other side of the object, say behind the object. The

same measurement and image reconstruction procedures are repeated. The resultant image is shown in Fig.3 (down). It is observed that the “smile” is changed to a “crying” in the image. By a correlation of these two images - each pixel intensities of the two images are multiplied by each other, the “smile” and the “crying” are canceled while the object image remains. The resultant image is shown in Fig.4 and it is clear that the artefact has been significantly suppressed.

V. CONCLUSIONS

Imaging of object in the near-field region using a modified UWB-SAR algorithm is presented. The “smile” artefact, which is inherited in the original algorithm, is effectively suppressed using the proposed procedures. The feasibility of the algorithm is demonstrated using experimental data. Future work will focus on better solutions to suppress such artefact using an algorithm for estimating the Direction of Arrival (DOA) of signals.

ACKNOWLEDGEMENT

This work has been supported by the Swedish research council VINNOVA via a project within the VINN Excellence centre CHASE.

REFERENCES

- [1] H. S. Lui and N. V. Z. Shuley, “Radar Target Recognition using a “Banded” E-Pulse Technique,” *IEEE Trans. Antennas and Propagat.*, vol. 54, no. 12, pp. 3874–3881, 2006.
- [2] Y. Wang, I. D. Longstaff, and C. J. Leat, “SAR Imaging of Buried Objects from MoM modelled scattered field,” *IEE Proc. Radar, Sonar and Navigation*, vol. 148, no. 3, pp. 167–172, 2001.
- [3] S. Vitebskiy, L. Carin, M. A. Ressler, and F. H. Le, “Ultra-Wideband, Short-Pulse Ground-Penetrating Radar: Simulation and Measurement,” *IEEE Trans. Geoscience and Remote Sensing*, vol. 33, no. 3, pp. 762–772, 1997.
- [4] J. Yang and A. Kishk, “A novel low-profile compact directional ultra-wideband antenna: the self-grounded Bow-Tie antenna,” *IEEE Trans. Antennas Propagat.*, vol. 59, accepted 2011.
- [5] —, “The self-grounded Bow-Tie antenna.” Spokane, Washington: 2011 IEEE AP-S International Symp. on Antennas Propag., 3-8 July 2011.

A.2 Paper B

UWB SAR Imaging of Near-Field Object for Industrial Process Applications

Seyedeh Shaghayegh Fayazi, Jian Yang and Hoi-Shun Lui

Paper accepted at the 7th European Conference on Antennas and Propagation
EuCAP 2013. The conference will be held in Gothenburg, Sweden, April 8-12,
2013.

UWB SAR Imaging of Near-Field Object for Industrial Process Applications

Seyedeh Shaghayegh Fayazi, Jian Yang, Hoi-Shun Lui,

Dept. of Signals and Systems, Chalmers University of Technology, SE-41296 Gothenburg, Sweden.
Email: sash0011@student.umu.se, jian.yang@chalmers.se, antony.lui@chalmers.se

Abstract—We present an aperture synthetic radar (SAR) system using ultra-wideband (UWB) signals for near-field object detection. An algorithm based on the Range Point Migration (RPM) method is used in the system. The results of this work clearly show that the UWB SAR accompanied with PRM can produce an image of an object free from undesired artifact from scattered field of adjacent antennas.

Index Terms—aperture synthetic radar, ultrawide-band, near-field imaging

I. INTRODUCTION

One of the promising near-field sensing techniques is ultra-wideband (UWB) aperture synthetic radar (SAR) system [1], [2]. However, one problem with SAR imaging algorithm in near-field sensing is that scattered fields from adjacent antennas produce a fault blurry image (referred to as artefact) around the true object. In [3], a simple solution to avoid the artifact was proposed. However, in more complex images, this simple solution cannot remove all artefacts.

In this study an algorithm based on Range Point Migration (RPM) is proposed to reduce such artefact. The RPM estimates an accurate Direction of Arrival (DOA) [4] to find an accurate target surface even for complex shaped target.

II. DATA ACCUSATION AND EXPERIMENTAL SETUP

The measurement setup consists of a self-grounded Bow-Tie antenna [5], [6] located in front of a rectangular metal plate. This metal plate then moves along a path of straight line of 1088 mm length. In order to achieve flexibility and accuracy in positioning this straight line is made of 68 Duplos LEGO Blocks with a length of 16 mm each block, shown in Fig.1. The distance between the antenna and the straight line is 715 mm. The monostatic response of each of these 68 positions is measured by Network Vector Analyzer (VNA) in frequency domain between 0.5 to 13 GHz, and then an inverse Fourier Transform is used to obtain the time domain data. All the measurements are recorded in an anechoic chamber so the reflection from surrounding environment is minimized.

III. IMAGING ALGORITHM PRINCIPLE

The SAR imaging technique is used to calculate the intensity of each pixel $I(m, n)$ by

$$I(m, n) = \sum_{k=1}^K S_k(t = T_{k,m,n}). \quad (1)$$

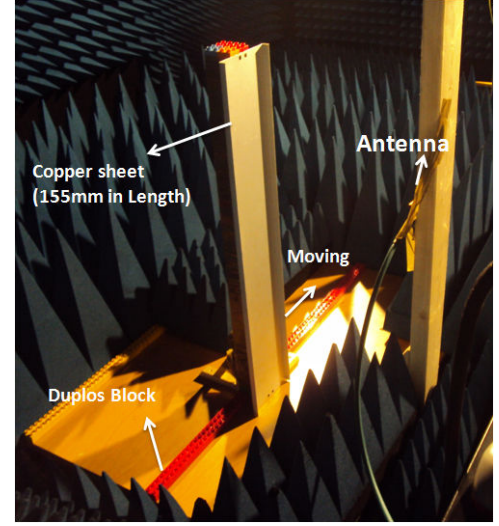


Fig. 1. Experimental setup.

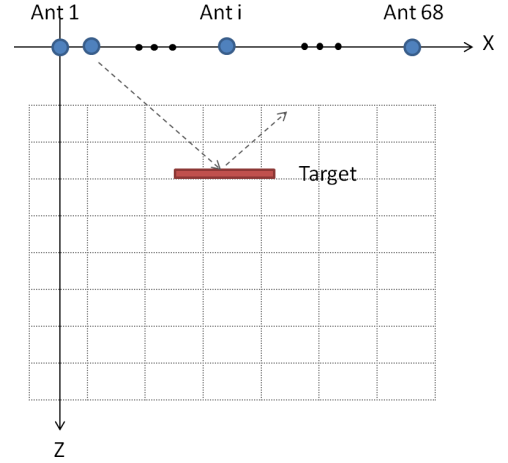


Fig. 2. The principle of the SAR algorithm.

where k is the total number of the antenna, S_k the received signal in time domain at the k_{th} antenna position and $T_{k,m,n}$ is the round-trip time delay between the k_{th} antenna and the physical position represented by pixel (m, n) in the image, as shown in Fig. 2. The SAR imaging algorithm provides the distance of the object where the signal is reflected.

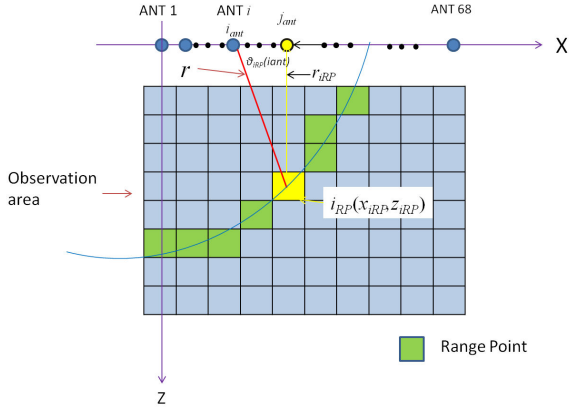


Fig. 3. The principle of RPM algorithm.

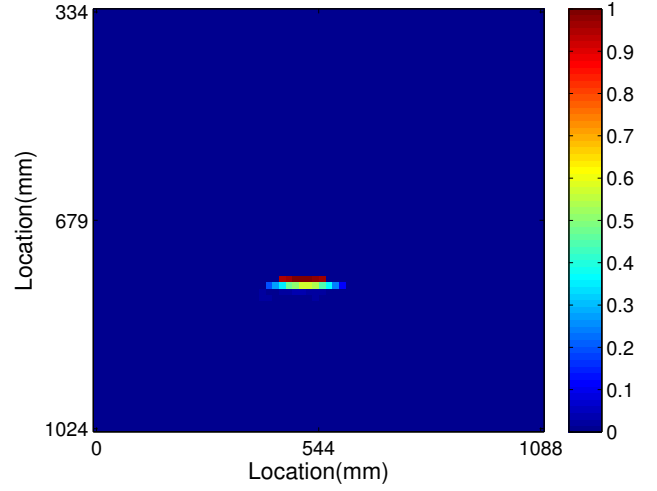


Fig. 5. Image reconstruction based on SAR-and-RPM combined algorithm.

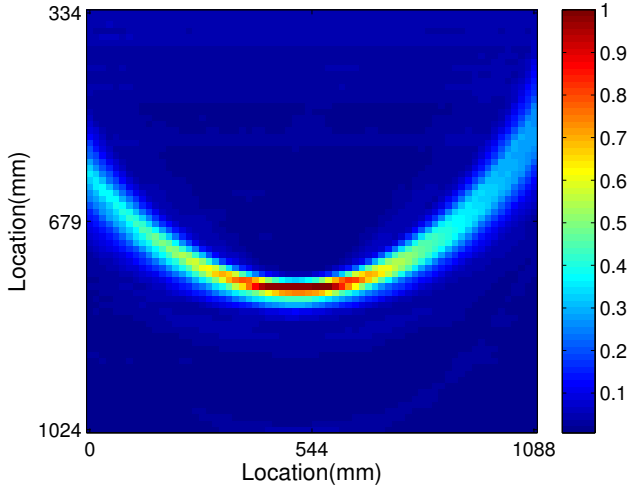


Fig. 4. Image reconstruction results based on SAR algorithm

Then, the Range Point Migration (RPM) method is used to estimate the Direction of Arrival (DoA). The principle can be presented in Fig. 3.

Combining the results from the SAR algorithm (the distance) and the RPM algorithm (the DoA), the location of the object where the signal is reflected can be determined.

IV. IMAGING RESULTS

Fig. 4 shows the imaging by using only SAR algorithm, and Fig. 5 shows the final imaging by using both SAR and RPM algorithms. It can be seen that the artefact can be removed by using the SAR-and-RPM combined algorithm.

V. CONCLUSION

The experimental data is used to demonstrate the capability of the SAR-and-RPM combined algorithm to remove artefact

in imaging. The details will be presented in the full paper. The technique can find many applications in industry, biomedical diagnosis and security, etc.

ACKNOWLEDGMENT

This work has been supported by CHASE Center at Chalmers University of Technology.

REFERENCES

- [1] Y. Wang, I. D. Longstaff, and C. J. Leat, "SAR Imaging of Buried Objects from MoM modelled scattered field," *IEE Proc. Radar, Sonar and Navigation*, vol. 148, no. 3, pp. 167–172, 2001.
- [2] S. Vitebskiy, L. Carin, M. A. Ressler, and F. H. Le, "Ultra-Wideband, Short-Pulse Ground-Penetrating Radar: Simulation and Measurement," *IEEE Trans. Geoscience and Remote Sensing*, vol. 33, no. 3, pp. 762–772, 1997.
- [3] S. Fayazi, H. Lui, and J. Yang, "Microwave imaging of near-field object using ultra-wideband synthetic aperture radar algorithm," *2012 IEEE International Symposium on Antennas and Propagation*, Chicago, USA, 8–14 July, 2012.
- [4] S. Kidera, T. Sakamoto, and T. Sato, "Super-Resolution UWB Radar Imaging algorithm Based on Extended Capon With Reference Signal Optimization," *IEEE Trans. Antennas and Propagation*, vol. 59, no. 5, pp. 1606–1615, 2011.
- [5] J. Yang and A. Kishk, "A novel low-profile compact directional ultra-wideband antenna: the self-grounded Bow-Tie antenna," *IEEE Trans. Antennas Propag.*, vol. 59, accepted 2011.
- [6] —, "The self-grounded Bow-Tie antenna." Spokane, Washington: 2011 IEEE AP-S International Symp. on Antennas Propag., 3–8 July 2011.

B

MATLAB Codes

B.1 Freq. Domain to Time Domain

```
for pp=1:n; %1 to 68, which measurement to choose
ff=ZDataALL(:,1,pp); %frequency points
fdata_real=ZDataALL(:,2,pp); %Real Part
fdata_imag=ZDataALL(:,3,pp); %Imaginary Part
fdata_real=fdata_real';
fdata_imag=fdata_imag';
fdata_real=[zeros(1,320), fdata_real];
fdata_imag=[zeros(1,320), fdata_imag];
%freq. 1.5MHz to 9GHz,
%to interpolate down to 0Hz roughly, two zeros are padded
NF_sample=length(fdata_real);%original frequency domain sample
%%% Bicycle window
f_max=9e9;
NF=1601+320;
d_f=f_max/NF;
f_min=d_f;
t_i=1/(6e9);
for i=1:NF
f = f_min+(d_f*(i));
w=2*pi*f;
B=exp((( -w))* t_i);
C(i)=((w*t_i)^4)*B;
end
```

```

f1=f_min:d_f:f_max;
fdata_real2=fdata_real.*real(C);
fdata_imag2=fdata_imag.*imag(C);
fr2 = [fdata_real2 , fliplr(fdata_real2(1:(NF_sample)))];
fi2 = [fdata_imag2(1:NF_sample),-fliplr(fdata_imag2(1:(...
NF_sample)))];
f_data2 = fr2 + j*fi2;
tdata2 = ifft(f_data2);
T_length= length(tdata2);
dt=1/(2*(f_max));
tt=0:dt:(T_length-1)*dt;
tt2=-((T_length-1)/2)*dt:dt:(0.5*(T_length-1))*dt;
t_old_ifft=tt2';
amp_old_ifft(:,pp)=20*log10(fftshift(tdata2))';
end

```

B.2 SAR Imaging

```

close all
clear all
clc
%% reading data im matlab
home_dir=[' '];
cd(home_dir);
load('Meas_1D_1A');
%% constatnt
c=2.9*1e+8;    % speed of light
Lego=0.016;    % lego component distance in m
pL=0.01;       % pixcel distance in m
res=0.016;
bb=2.3*1e-9;   % time gating
default_z=0.5*c*bb;
n=68           %Number of positions
Nx=68;         %Number of pixels
Ny=68;         %Number of picels;
Nk=68          %Number of Antennas
%% Preprocessing
for i=1:n;
t=MeasALL_R_1D(:,1,1);
amp=MeasALL_R_1D(:,2,i);
y=(10).^(amp./10);
MeasAll_L(:, :, i)=[t,y];    % raw data in linear

```

```

x=log10(y);
t_ann=MeasALL_AR(:,1);
amp_ann=MeasALL_AR(:,2);
y_ann=(10).^(amp_ann./10);
y_imp=abs(y-y_ann);
Sub_amp=10*log10(y_imp);
MeasAll_subtract_dB(:, :, i)=[t, Sub_amp];
MeasAll_subtract_L(:, :, i)=[t, y_imp];
index=find(t==bb);
tnew=t(index:end);
AmpNew=y_imp(index:end);
AmpNew_dB=Sub_amp(index:end);
AmpNew_rawdata=y(index:end);
MeasAll_improved_timegating(:, :, i)=[tnew, AmpNew];
MeasAll_timegating_dB(:, :, i)=[tnew, AmpNew_dB];
MeasAll_rawdata_L(:, :, i)=[tnew, AmpNew_rawdata];
i;
end
%% SAR Imaging Algorithm
for i=1:n
    Amp_Imp(:, i)=MeasAll_rawdata_L(:, 2, i);
    end
    for k=1:Nk
        for j=1:Nx
            for i=1:Nz
                D(k, j, i)=sqrt(((default_z)+(i-1)*pL)^2+(((k*Lego)-(j*res))^2));
            end
        end
    end
    tid=((D)*2)./c;
    for i=1:Nz
        for j=1:Nx
            Sum=0;
            for k=1:Nk
                [min_difference, Indx] = min(abs((tnew-tid(k, j, i))));
                dummy=Amp_Imp(Indx, k);
                Sum=Sum+dummy;
            end
            Image_Final(i, j)=Sum;
        end
    end
end
figure ,

```



```

imagesc(Image_Final);
title('constructed image in Linear ');
colorbar;
NImage_Final=(Image_Final(:,:))./max(max(Image_Final(:,:)));
imagesc(NImage_Final);
colorbar;
title('Normalized constructed image in Linear ');
imagesc(10*log10(NImage_Final));
title('Reconstructed SAR image in dB');
colorbar;

```

B.3 DOA Method

```

% DOA
% x res=0.016m , z res=0.01m
close all
clear all
clc
tic
%% reading data in matlab
home_dir=[' '];
cd(home_dir);
load('Meas_1D');
%% constant
n=68; % number of positions
Lego=0.016; % distance between antenna
N_ant_start=1;
N_ant_end=68;
N_x=68; %number of pixel in x direction
N_z=68; %number of pixel in z direction;
size_x=(N_ant_end-N_ant_start)*Lego;% x direction
size_z=size_x; % z direction
res=0.016; %size_x/(N_x-1); % distance in x direction
pL=0.01; %size_z/(N_z-1); % distance in z direction
%% constant
c=2.9*1e+8; % speed of light
bb= 2.3*1e-9; % time gating
N_sample=6401; % number of samples
N_sample_timegate=2465;%number of samples after time gating
Nj_start=1; %j=x direction number of columns
Nj_end=N_x;
Ni_start=1; %i=z direction number of rows

```

```

Ni_end=N_z;
default_z=0.5*c*bb;
Sigma_x=10;          % constant in DoA function
Sigma_theta=pi ;    %pi/50; constant in DoA function

%% raw data ,subtracted data and timegating in linear and dB
MeasAll_rawdata_L=zeros ( N_sample_timegate ,2 ,n);
for i=1:n;
t=MeasALL_Y_1D (: ,1 ,1);
amp=MeasALL_Y_1D (: ,2 ,i );
y=(10).^(amp./10);
index=find ( t==bb );
tnew=t ( index :end );
AmpNew_rawdata=y ( index :end );
MeasAll_rawdata_L (: ,: ,i )=[tnew ,AmpNew_rawdata ];
    i ;
end
%%
amplitude=zeros ( N_sample_timegate ,n);
for i=1:n
amplitude (u ,i)=MeasAll_rawdata_L (: ,2 ,i );
end
D=zeros (n ,N_x ,N_z );
theta_physical=zeros (n ,N_x ,N_z );
for k=N_ant_start :N_ant_end
for j=Nj_start :Nj_end
for i=Ni_start :Ni_end
D(k ,j ,i)=sqrt ( ((( default_z)+(i-1)*pL)^2+(((k*Lego)...
-(j*res))^2));
theta_physical(k ,j ,i)=atand ( ((( default_z)+(i-1)*pL)...
/((j*res)-(k*Lego)));
if theta_physical(k ,j ,i)<0
theta_physical(k ,j ,i)=theta_physical(k ,j ,i)+90;
else
theta_physical(k ,j ,i)=theta_physical(k ,j ,i);
end
end
end
end
tid=(((D)*2)./c);
theta_vec=linspace (0 ,180 ,180);
theta_man=zeros (n ,N_x ,N_z );

```

```

val=zeros(n,N_x,N_z);
physical_Val=zeros(n,N_x,N_z);

for i=Ni_start:Ni_end
for j=Nj_start:Nj_end
Sum=0;
Sum_UWB=0;
% if Image_Final_UWB(i,j)==0
% Image_Final_UWB(i,j)=0;
% else
for k=N_ant_start:N_ant_end
radius_ref=D(k,j,i);
radius_all=D(k,:,:) ;
[s_jant,X,THETA,theta_RP,N_RP_NZ]=maxopt_1(k,radius_all,...
radius_ref,tnew,tid,amplitude,Lego,res,pL,Nj_start,Nj_end...
,Ni_start,Ni_end,default_z,Sigma_x,N_sample_timegate);
%[theta_opt(k,j,i),fval]=fminbnd(@(theta)-max_value(s_jant...
%,X,THETA,theta,Sigma_theta),0,180);
[val(k,j,i),theta_man(k,j,i),Max_Vec]=optimal_theta(s_jant...
,X,THETA,theta_vec,Sigma_theta);
physical_Val(k,j,i)=physical_theta(s_jant,X,THETA...
,theta_physical(k,j,i),Sigma_theta);
[min_difference_UWB, Indx_UWB] = min(abs((tnew...
(1:N_sample_timegate,:)-tid(k,j,i))));
dummy_UWB= amplitude(Indx_UWB,k);
Weg_UWB=dummy_UWB*(exp((physical_Val(k,j,i))...
/(val(k,j,i))));
Sum_UWB=Sum_UWB+Weg_UWB;
end
Image_Final_UWB(i,j)=Sum_UWB;
end
x_ant=zeros(1,n);
x_RP=zeros(1,n);
theta_RP=zeros(1,n);
end
i
end
figure(1),
imagesc(Image_Final_UWB);
title(strcat('Reconstructed image (',num2str(N_x),...
' x ',num2str(N_z),' pixel')'));
colorbar;

```

```

NImage_Final_UWB=(Image_Final_UWB(:,:))./max(max ...
(Image_Final_UWB(:,:)));
figure(2),
imagesc(NImage_Final_UWB);
title(strcat('Normalized Reconstructed image(', ...
num2str(N_x),'x',num2str(N_z),'pixel')'));
colorbar;
Image_Final_UWB_db(:,:)=10*log10(NImage_Final_UWB(:,:));
figure(3)
imagesc( Image_Final_UWB_db);
colorbar;
toc

```

B.4 Optimal Theta

```

function [val,theta_man,Max_Vec]=optimal_theta ...
(s_jant,X,THETA,theta_vec,Sigma_theta)
for p=1:180
Max_Vec(1,p)=(abs(sum(s_jant.*exp(-(X+(((theta_vec(1,p)...
-THETA).^2)/(2.*((Sigma_theta)^2))))))));
end
[val ind]=max(Max_Vec);
theta_man=theta_vec(ind);

```

B.5 Physical Theta

```

function physical_Val=physical_theta(s_jant,X,THETA,...
theta_physical,Sigma_theta)
physical_Val=(abs(sum(s_jant.*exp(-(X+(((theta_physical...
-THETA).^2)/(2.*((Sigma_theta)^2))))))));

```

B.6 RPM Method

```

function [s_jant,X,THETA,theta_RP,N_RP_NZ]=maxopt_1(k,radius_...
all,radius_ref,tnew,tid, amplitude,Lego,res,pL,Nj_start,...
Nj_end,Ni_start,Ni_end,default_z,Sigma_x,N_sample_timegate)
N_RP=0;
N_RP_NZ=0;
radius_min=(radius_ref-0.001);
radius_max =(radius_ref+0.001);
for n=Nj_start:Nj_end % n=j number of columns
for m=Ni_start:Ni_end % m=i number of rows

```

```

radius=radius_all(1,n,m);
if radius_min<=radius && radius<=radius_max
N_RP=N_RP+1;
N_RP_NZ=N_RP_NZ+1;
x_ant(1,N_RP)=(k-1)*Lego;
x_RP(1,N_RP)=(n-1)*res;
theta_RP1(1,N_RP)=atand(((m-1)*pL+(default_z))./(...
(n*res)-(k*Lego)));
if theta_RP1(1,N_RP)<0
theta_RP1(1,N_RP)=theta_RP1(1,N_RP)+90;
else
theta_RP1(1,N_RP)=theta_RP1(1,N_RP);
end
[M I]=min(tid(:,n,m));
[ min_difference , Indx ] = ...
min(abs(((tnew(1:N_sample_timegate,:)-(tid(I,n,m)))))));
s_jant(1,N_RP)= amplitude(Indx,I);
THETA1(1,N_RP)=theta_RP1(1,N_RP);
else
N_RP=N_RP+1;
x_ant(1,N_RP)=0;
x_RP(1,N_RP)=0;
theta_RP1(1,N_RP)=0;
s_jant(1,N_RP)=0;
THETA1(1,N_RP)=0;
end
end
end
X=((x_ant-x_RP).^2)./(2*((Sigma_x)^2));
THETA=THETA1;
theta_RP=theta_RP1;

```

B.7 Scattered Field

```

function f=max_value(s_jant,X,THETA,theta,Sigma_theta)
f=(abs(sum(s_jant.*exp(-(X+(((theta-THETA).^2)./(...
(2.*((Sigma_theta)^2))))))));

```